Bioinspired Microgel-loaded Smart Membrane Filtration with Thermo- and Ion- Dual Responsive Water Gate for Selective Lead(II) Separation

Botuo Zheng[a,#], Bingnan Zhou[a,#], Jing Hu[a], Cun-ai Zheng[a], Kaixuan Chen[a], Shuai Yang[a], Walter Richtering[b], David Harbottle[c], Timothy N. Hunter[c], Huagui Zhang[a,*]

[a] College of Chemistry and Materials Science, Fujian Province Key Laboratory of Polymer Science, Fujian Normal University, Fuzhou, 350007, China

[b] Institute of Physical Chemistry, RWTH Aachen University, Landoltweg 2, 52056 Aachen, Germany, European Union

[c] School of Chemical and Process Engineering, University of Leeds, Leeds LS2 9JT, UK

[#] the authors equally contributed to this work.

Abstract: Pb^{2+} is a ubiquitous pollutant. Membrane filtration represents one of the common water treatment techniques, but the fixed pore size larger than ion and the non-affinity to ions of membrane hamper direct separation of Pb^{2+} without tedious operations. Herein, inspired from the Pb^{2+}-tolerable oleander that enriches and intercepts Pb^{2+} in roots from permeating to plant body, a smart Pb^{2+}-adsorptive filtration membrane with a temperature- and ion-tunable water gate was prepared by loading dual-responsive poly(*N*-isopropylacrylamido-*co*-acrylamido-benzo-18-crown-6) (PNB-5-20) microgels on a commercial membrane. The PNB-5-20 microgel exhibits pronounced temperature-responsive swelling/de-swelling (650 nm to 330 nm) with a volume phase transition temperature (VPTT) around 33 °C. Moreover, the microgel shows a high Pb^{2+}-adsorption capacity (q_{max}, 85.4 mg/g) and good selectivity (distribution coefficient K_d ~ 1000 mL/g) thanks to the complexation of crown ether, as well as good Pb^{2+} responsiveness, having the VPTT positively shifted to 40 °C in the presence

of Pb^{2+} with enhanced swelling behaviors. Functionalized with PNB-5-20, the smart membrane integrates Pb^{2+} detection, adsorption and tunable water drainage in a single device. The membrane selectively recognizes Pb^{2+} in the polluted water with the gates in membrane pores switch from "open" to "closed", intercepting and adsorbing Pb^{2+} with water permeation retarded. Once purified, the gates can be facilely "re-opened" by increasing the temperature. Construction of such an intelligent membrane filtration device with tunable water gate, excellent Pb^{2+} recognition and adsorption performance will greatly simplify the remediation of Pb^{2+}-polluted water.

Keywords: lead(II), microgel, membranes, adsorption, crown ether, *N*-isopropylacrylamide.

1. Introduction

Water contamination by heavy metals (e.g., Cd^{2+}, Cr^{6+}, Cu^{2+}, Hg^{2+}, and Pb^{2+}) is a major environmental problem worldwide and it is imperative that cost effective and sustainable solutions can be developed.[1] Among the contaminants, Pb^{2+} is both one of the most common and also toxic heavy metal ions.[2-6] Various industrial processes, such as battery productions, mining, paints and metal plating,[3-5, 7, 8] release Pb^{2+} to the environment, and Pb^{2+} pollution is also aggravated by the extensive use and waste of lead-containing products, such as leaded gasoline, military weapons and cosmetics.[3, 9, 10] However, as a naturally existing element, non-degradable ion, Pb^{2+} has good water solubility and affinity to proteins, which make it readily absorbed by terrestrial and aquatic organisms. Its eventual accumulation in the human body through drinking water and the food chain [11-13] can lead to serious damage to the nervous system, immune system, and kidneys,[2, 7, 14] especially affecting the intellectual development of children. [15, 16] Therefore, effective removal of Pb^{2+} from the aqueous environment is urgent and important in practice, and thereby has attracted great research interest.

So far, several technologies have been developed for the removal of Pb^{2+} from

water, such as chemical precipitation,[17] ion exchange,[18] membrane separation,[19] photocatalytic [20] and adsorption.[3, 21] Adsorbent sorption represents one of the most popular treatment methods for various ions besides Pb^{2+},[22-24] but often conflicted by the difficulty in recovering the particulate adsorbents that may cause secondary pollution to the environment.[25-27]

Membrane purification is a common separation technique widely used in water treatment thanks to its high flexibility, easy scalability, and low energy consumption.[28-33] In particular, nanofiltration membranes [34] are extensively used in separation of metal ions like Pb^{2+} via size exclusion of dense micro-structures [35] or electrostatic interaction arising from introduced positive charges.[36-38] Ultrafiltration membranes with adsorbents [39] incorporated are also effective devices that can efficiently remove Pb^{2+} from polluted water.[40-43] However, both the nanofiltration and ultrafiltration membranes usually require high transmembrane pressure to drive water during filtration regardless of whether the target species exist in the water. This may result in the waste of energy when the membranes are deployed without the prior knowledge about the water quality. The need for pressurization also limits the application of the membranes in some cases such as portable devices for emergency or daily life, while microfiltration membranes with larger pores are weak at intercepting polluted water. A membrane device that can recognize the polluted and clean water, and then selectively drain the clean water while retard the polluted solution, is of great worth in practical applications.

Nerium oleander L. (oleander) has been demonstrated as a plant bio-detector that not only can grow in Pb^{2+}-polluted soils but also is good at remedying Pb^{2+} [44]. Investigations on the compositions of different parts of the plant revealed that the Pb^{2+} are enriched in the roots of oleander [45, 46] but is less so in other parts. Interestingly, once adsorbed in the root, the transfer of Pb^{2+} to the shoots of the plant is interfered with declined water flux, giving low Pb^{2+} concentration and thus low Pb^{2+} toxicity in leaves where active proteins functions. The Pb^{2+}-interception and enrichment

mechanisms by oleander root displays an ion-responsive characteristic from a membrane perspective, that is, the membrane permeability decreases as Pb^{2+} is detected and adsorbed. This inspires us to develop a similar smart adsorptive filtration membrane with tunable water gating system that can recognize $Pb^{2+}$and responsively regulate the gate to hinder water permeation and simultaneously adsorb the Pb^{2+} in the membrane before purified water allowed to pass the membrane.

Macrocyclic crown ethers are well known to possess outstanding affinity to metal ions due to their excellent solvation ability and regular electron-donating domains [47]. In particular, the 18-crown-6 ether (18C6) can selectively bind Pb^{2+} with a high equilibrium constant (log K ~ 7) higher than that of common competing ions such K^+ and Na^+ (4~6) [47] regardless of the solvents, i.e., chemical environments [48]. Moreover, the derivatives of 18C6 including benzo-18-crown-6 ether or cylcohexano-18-crown-6 ether exhibit both good hydrophilicity and good oleophilility, allowing it to be modified or applied in multi-solvent and multi-phase system [49]. The features make 18C6 an excellent building block as adsorption sites in establishing the smart adsorptive filtration device simulating oleander root.

Here, to simulate the oleander root to separate Pb^{2+} in one-step based on an integrated device to avoid tedious operations, a smart filtration membrane was prepared by loading a Pb^{2+}- and temperature- dual responsive microgel on a commercial Nylon membrane to establish a tunable water gating system in response to environment changes. The dual responsive microgel, poly(*N*-isopropylacrylamido-*co*-acrylamido-benzo-18-crown-6) (PNB-5-20), was designed using *N*-isopropylacrylamide (NIPAm) as thermo-responsive domains and benzo-18-crown-6 (B18C6) as Pb^{2+} recognizer/adsorbent. The microgels swell below volume phase transition temperature (VPTT) while collapse above and the VPTT positively shifts by ~ 7 °C when Pb^{2+} is present. Hence, in a specific temperature range, Pb^{2+} can trigger swelling of the collapsed or less swollen microgel, enabling function of a smart water gating system in the microgel loaded Nylon membrane with

the gates in the membrane pores spontaneously switch from an “open” to a “closed” state by recognizing Pb^{2+} in the environment. Thus, Pb^{2+}-polluted water can be retained before the membrane and continuously adsorbed by the microgels until the water is purified. Moreover, its thermo-responsiveness enables the “closed” gates in the smart membrane to “re-open” promptly via heating to release the purified water. The bio-inspired fabrication of the smart membrane combines Pb^{2+} detection and adsorption as well as the controllable retaining and drainage of water in a solo device, exhibiting great advantage of low energy-consumption and high efficiency in processing Pb^{2+}-polluted water.

2. Experimental section

2.1. Materials

N-isopropylacrylamide (NIPAm, 98%), benzo-18-crown-6 (B18C6, 95%), acryloyl chloride (≥ 98%), 10% Pd/C, $CDCl_3$, D_2O, *N,N’*-Methylene-bis-acrylamide (BIS, ≥ 99%), cetyltrimethylammonium bromide (CTAB, 99%), 2,2'-azobis(2-Methylpropionamidine) dihydrochloride (AIBA, ≥ 98%) were purchased from Adamas-beta. Dichloromethane (AR), glacial acetic acid (AR), concentrated nitric acid (AR), anhydrous magnesium sulfate (AR), anhydrous ethanol (AR), 2-methoxyethanol (≥ 99%), hydrazine hydrate (AR), triethylamine (≥ 99%), tetrahydrofuran (THF, ≥ 99.5%), methanol (AR), column chromatography silica gel, $Pb(NO_3)_2$ (AR), KNO_3 (AR), $NaNO_3$ (AR), $CsNO_3$ (AR), Na_2CO_3 (AR), KBr (AR), $MgCl_2·6H_2O$ (≥ 98%), $CaCl_2$(> 96%) were purchased from Sinopharm Chemical Reagent Co Ltd. All the reagents were used as received.

2.2. Preparation of smart filtration membrane loaded with dual responsive PNB-5-20 microgels

2.2.1. Synthesis of 4-Acryloylamidobenzo-18-crown-6 (BCAm)

BCAm was synthesized based on B18C6 according to a three-step method reported in the literature [50, 51]. In particular, B18C6 was first nitrified into nitrobenzo-18-crown-6 (N-B18C6). 2.0 g B18C6 was dissolved in dichloromethane, and then a mixed solution of 7.0 mL concentrated nitric acid and 24.0 mL glacial acetic acid was added dropwise. The mixture was stirred at 25 °C for 24 h for reaction. At the end of the reaction, the residual nitric acid was neutralized with saturated sodium carbonate solution, and the oil phase was separated from aqueous phase by a separatory funnel. The organic phase was then dried with anhydrous magnesium sulfate, which was removed by filtration later. The filtrate was then concentrated under vacuum, and the product N-B18C6 was collected by recrystallization from its ethanol solution under -18 °C. (Yield 2.1 g, 91%). ^{1}H NMR δ: 7.88 ppm (dd, 1H, J = 8.9, 2.6 Hz), 7.73 ppm (d, 1H, J = 2.6 Hz), 6.88 ppm (d, 1H, J = 8.9 Hz), 4.26–4.20 ppm (m, 4H, -OCH_2-CH_2O-), 3.98–3.92 ppm (m, 4H, -OCH_2-CH_2O-), 3.80–3.65 ppm (m, 12H, -OCH_2-CH_2O-).

Secondly, the N-B18C6 was reduced into aminobenzo-18-crown-6 (A-B18C6). 0.5 g of the as-prepared N-B18C6 was dissolved in 2-methoxyethanol, and 8.75 mL hydrazine hydrate was added as reducing agent with 0.05 g 10% Pd/C as the catalyst. The reaction was performed at 70 °C under nitrogen atmosphere for 2 h. At the end of the reaction, the solid catalyst was removed by filtration. The filtrate was concentrated by rotary evaporation, diluted with water and extracted against DCM sequentially. The oil phase was then collected and dried with anhydrous magnesium sulfate. The solvent in the filtrate was removed under vacuum to give a light yellow oil. The product was identified to be A-B18C6. As an intermediate containing a benzylamine moiety, the A-B18C6 is susceptible to oxidation and turns brown gradually during

storage. Therefore, the as-prepared A-B18C6 needs to be subjected to following amidation as soon as possible. (Yield 0.4534 g, 97%). ^{1}H NMR δ: 6.72 ppm (d, 1H, *J* = 8.4 Hz), 6.28 ppm (d, 1H, *J* = 2.6 Hz), 6.21 ppm (dd, 1H, *J* = 8.4, 2.6 Hz), 4.08 ppm (m, 4H, -OCH_2-CH_2O-, *J* = 9.6, 5.5, 4.0 Hz), 3.89 ppm (m, 4H, -OCH_2-CH_2O-, *J* = 18.7, 5.4, 4.0 Hz), 3.77–3.67 (m, 12H, -OCH_2-CH_2O-).

Lastly, A-B18C6 was acylated into BCAm, the target molecule. The 0.4 g prepared A-B18C6 was dissolved in 10 mL THF followed by 0.16 mL acryloyl chloride as the acylation reagent and 0.3 mL triethylamine as the proton scavenger. The vessel was sealed and the reaction was carried out at 4 °C for 1.5 h and at room temperature for the subsequent 24 h. After completion of the reaction, the insoluble salts produced were removed by filtration. As the solvent in the filtrate was removed under vacuum, the residues were diluted by water and extracted against DCM. Then the oil phase was collected and dried with anhydrous magnesium sulfate. The crude product was obtained after removal of DCM under vacuum. Finally, the BCAm was refined by column chromatography using MeOH/DCM = 1:20 as the eluent, and a dry mass of white powder can be obtained, which is stable during storage. (Yield 0.4543 g, 97~~.48~~%) ^{1}H NMR δ: 7.63 ppm (s, 1H, -CO-NH-), 7.45 ppm (d, 1H, *J* = 2.3 Hz), 6.92 ppm (dd, 1H, *J* = 8.6, 2.3 Hz), 6.79 ppm (d, 1H, *J* = 8.6 Hz), 6.40 ppm (dd, 1H, CH_2=CH-, *J* = 16.8, 1.4 Hz), 6.25 ppm (dd, 1H, CH_2=CH-, *J* = 16.8, 10.1 Hz), 5.72 ppm (dd, 1H, CH_2=CH-, *J* = 10.1, 1.4 Hz), 4.16–4.08 ppm (m, -OCH_2-CH_2O-, 4H), 3.89 ppm (m, -OCH_2-CH_2O-, 4H, *J* = 9.2, 5.3 Hz), 3.78–3.64 ppm (m, -OCH_2-CH_2O-, 12H).

2.2.2 Preparation of poly(*N*-isopropylacrylamido-*co*-acrylamido-benzo-18-crown-6) (PNB-5-20) microgels

PNB-5-20 microgel was synthesized in one step by precipitation copolymerization of NIPAM and the as-prepared BCAm using BIS as the cross-linking agent. As a typical synthesis of PNB-5-20, NIPAm (230.9 mg, 2 mmol),

187 BCAm (157.3 mg, 0.4 mmol), BIS (18.5 mg, 0.12 mmol), and 5 mg CTAB were first
188 dissolved in100 mL deionized (DI) water contained in a three-necked flask. The flask
189 was purged with nitrogen to exclude oxygen, and then the system was heated to 70 °C
190 under nitrogen purge for 30 min. Subsequently, polymerization was initiated by
191 adding 7.7 mg AIBA dissolved in 1 mL deionized water into the solution dropwise
192 with a syringe. The reaction was kept at 70 °C under nitrogen atmosphere for 5 h. At
193 the end of the reaction, the mixture was cooled to room temperature under continued
194 stirring. The microgel products were collected by centrifugation at 8000 rpm and
195 washed by deionized water for three times to remove unreacted monomers. The yield
196 of PNB-5-20 is about 238 mg, 60%. The purified microgels were dispersed in
197 deionized water for storage. For comparison purpose, neat PNIPAm microgel was
198 synthesized according to the identical procedure but in the absence of BCAm. Table 1
199 lists the formulations for the synthesis of PNB-5-20 and PNIPAm microgels.
200
201 Table 1. The quantities of feedstocks used in the synthesis of PNB-5-20 and neat PNIPAm
202 microgels.

Sample	NIPAm	BCAm (relative to NIPAm)	BIS (relative to monomers)	CTAB	AIBA (relative to monomers)	H_2O
PNB-5-20	2 mM	20 mol%	5 mol%	1.37×10^{-4} mol/L	2 wt%	100 mL
PNIPAm	2 mM	/	5 mol%		2 wt%	100 mL

203 2.2.3 Preparation of microgel-loaded membranes

204 Figure 1 illustrates the fabrication of a PBN-5-20 microgel-loaded membrane
205 and its dual-responsiveness towards the temperature and Pb^{2+}. Commercially
206 available nylon 6 membrane (pore size 0.45 μm, diameter 25 mm) was selected as the
207 carrier membrane, which was assembled in a vacuum filtration device connected to a
208 vacuum pump. Then, 1 mL PNB-5-20 microgel dispersion in deionized water (solid
209 content 1.2 g/L) was filtered through the vacuum filtration device, whereby the
210 PNB-5-20 microgels were loaded onto the nylon 6 membrane by pressure. After the

filtration, the decorated membrane was air-dried at room temperature and stored for subsequent use.

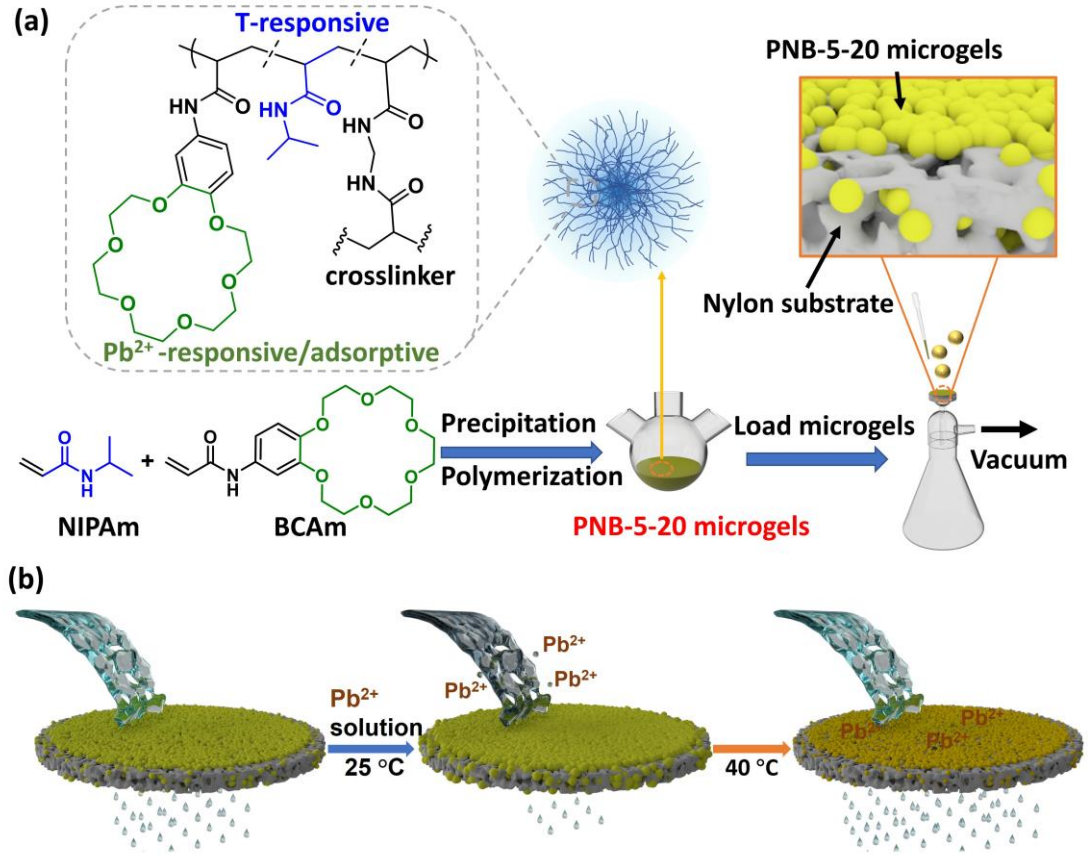

Figure 1. (a) Structure of PNB-5-20 microgel and the preparation of a PBN-5-20 microgel-loaded membrane and (b) its dual responsiveness to temperature and Pb^{2+}.

2.3. Characterizations

2.3.1. Nuclear Magnetic Resonance (NMR)

The ^{1}H NMR spectra of B18C6, N-B18C6, A-B18C6, and BCAm monomers as well as PNB-5-20 microgels were obtained on a Bruker AV 400 M NMR spectrometer using $CDCl_3$ or D_2O as the solvent.

2.3.2. Fourier Transform Infrared (FT-IR)

A Nicolet IS50 Fourier transform infrared spectrometer (Thermo Scientific) was used to characterize the chemical composition of dried PNIPAm and PNB-5-20 microgels. The samples were prepared by the KBr tablet method. Each sample was

scanned 32 times at a resolution of 4 cm^{-1} in the range of 400 cm^{-1} to 4000 cm^{-1} and the average signal was used.

2.3.3. Dynamic Light Scattering (DLS)

The hydrodynamic diameters of PNIPAm and PNB-5-20 microgels in pure water or solutions containing inorganic metal ions were measured according to the Stokes-Einstein equation using a NANOSIZER (Malvern) at different temperatures. The measurement in each temperature was carried out after the dispersion was stabilized at the designated temperature for 180 s and the number of measurements was set to three.

2.3.4. Inductively Coupled Plasma-Optical Emission Spectroscopy (ICP-OES)

The Pb^{2+} concentration in the solution before and after adsorption was measured using the ICP-OES (Optima 8000, PerkinElmer) at a specific emission wavelength of 220.353 nm for lead(II) ions. The Pb^{2+} concentrations in the samples were diluted to the range of 0-1 ppm and filtered through a 0.22 μm poly(ether-Sulfone) filter prior to testing.

2.3.5. Scanning electron microscopy (SEM) and energy dispersive X-ray spectroscopy (EDX) mapping

The morphology of PNIPAm and PNB-5-20 microgels was observed by SEM (Sigma 300, ZEISS) coupled with EDX. First, a drop of the microgel dispersion was placed on a clean silicon substrate. After being dried in the air at room temperature, the sample was sprayed with gold and then observed under an accelerating voltage of 7.0 kV. For membrane samples, the dried membranes were directly gold sprayed and then observed under SEM. An X-ray spectrometer combined with SEM was used to analyze the elemental maps of samples with a current of 10 μA and an accelerating voltage of 10.0 kV.

250 2.3.6. X-ray photoelectron spectroscopy (XPS)

251 Chemical compositions and bonding information of the samples were analyzed
252 using an XPS (K-Alpha, Thermo Scientific) system. An electron/ion gun was used to
253 compensate the charge accumulation on the sample during the measurement. XPS
254 peaks were fitted using Avantage software and the binding energy was corrected by C
255 1s photoelectron at 284.8 eV as reference.

256 2.4. Pb^{2+} adsorption

257 2.4.1. Adsorption isotherms

258 The adsorption isotherms of PNB-5-20 and PNIPAm microgels were determined
259 at different Pb^{2+} concentrations (10, 40, 60, 100, 300, and 500 ppm) with a solid
260 content of 0.75 g/L. The mixture of the microgel and Pb^{2+} solution was shaken at
261 room temperature and 120 rpm for 24 h. Afterwards, the PNB-5-20 microgel was
262 removed by filtration through a 50 nm nylon 6 membrane. The residual Pb^{2+}
263 concentration in the filtrate was determined by ICP-OES. The PNIPAm microgel was
264 used as reference and its adsorption isotherm was determined based on the same
265 procedure. The equilibrium adsorption capacity q_e (mg/g) was calculated by Equation
266 (1):

267 $$q_e = \frac{(C_0 - C_e)V}{m} \quad (1)$$

268 where C_0 (mg/L) and C_e (mg/L) are the initial and equilibrium concentrations of Pb^{2+}
269 in the mixture, respectively; m (g) is the mass of the microgel and V (L) is the volume
270 of the mixture.

271 2.4.2. Adsorption kinetics

272 The adsorption kinetics of Pb^{2+} on PNB-5-20 microgels was tested at an initial
273 Pb^{2+} concentration of 100 ppm with a solid content of 0.75 g/L. The dispersions were
274 shaken at 120 rpm for 10, 20, 30, 60, 180, 360, and 1440 min, respectively, at room
275 temperature in a series of 10 mL plastic centrifuge tubes. Afterwards, the samples

were filtered through 50 nm nylon 6 membranes to remove microgels, and the Pb^{2+} concentration in the filtrate was determined by ICP-OES. PNIPAm microgels was used as a control sample to compare the adsorption kinetics based on the same procedure. The adsorption capacity q_t (mg g^{-1}) was calculated according to Eq (2):

$$q_t = \frac{(C_0 - C_t)V}{m} \quad (2)$$

where C_t (mg L^{-1}) is the concentrations of Pb^{2+} at any moment during the adsorption.

2.4.3. The effects of pH and temperature

The effect of pH was investigated based on Pb^{2+} adsorption experiments carried out with C_0 = 100 ppm and solid content: 0.75 g/L in solutions with varied pH ranging from 2 to 10. The pH was adjusted with 0.1 mol/L HCl and 10^{-3} mol/L NaOH solutions. Likewise, the effect of temperature was investigated based on adsorption experiments of PNB-5-20 microgels at temperatures ranging from 25–40 °C in Pb^{2+} solutions with C_0 = 20 ppm.

2.4.4. Effect of competitive ions

The selectivity of PNB-5-20 microgels towards Pb^{2+} in the presence of competing ions was investigated at a solid content of 0.75 g/L in mixtures containing Pb^{2+} (10 ppm) and Na^+, K^+, Ca^{2+}, or Mg^{2+} at different concentrations (100, 200, 400, and 800 ppm). The mixtures were shaken at 120 rpm for 24 h at room temperature and then filtered through a 50 nm nylon 6 membrane, and the concentration of Pb^{2+} in the filtrate was determined by ICP-OES.

2.4.5. Membrane filtration test

To simulate the practical application and to evaluate the responsive water-gating function of the smart microgel-loaded membrane, a sequential filtration experiment was performed based on a laboratory-scale membrane filtration device shown in Figure 2. The as-prepared nylon 6 filter membrane loaded with PNB-5-20 microgel was immobilized in a replaceable membrane filter unit made of PP (effective diameter

22 mm). Then, the filter unit was placed in a water bath thermostat with both of the filter heads connected to silicone tubes, through which the sample liquid (i.e., the DI water or Pb^{2+} solutions) was circulated to the filtration membrane as driven by a peristaltic pump. The permeability performance of the membrane was first tested, in term of liquid flux per 2 min, with DI water and with the temperature set to 25 °C by the water bath.

5.9 mL DI water in PE vial was pumped through the membrane via peristaltic pump at a flow rate of 1 mL/min, and the filtrate was collected in a volumetric cylinder with the fluxes recorded every 2 min. After the test, the filtrate was transferred back into the vial holding the eluent for circulation.

After a period of time, 0.1 mL of $Pb(NO_3)_2$ solution (30 mM) was added to the PE vial to obtain a 0.5 mM Pb^{2+} solution. The Pb^{2+} solution was allowed to circulate through the filter membrane under the drive of the peristaltic pump. The volume of the filtrate was recorded every 2 min to monitor the permeability change of the membrane as Pb^{2+} was recognized and adsorbed by the membrane, and the filtrate was transferred back to the PE vial. Moreover, to evaluate the purification efficiency the Pb^{2+} concentration in the PE vial was monitored throughout the circulation process by taking 0.05 mL liquids every 2 min for ICP-OES analysis. Once the adsorption equilibrium was reached based on the adsorption kinetics data, the water bath temperature was adjusted to 40 °C to check its temperature-responsive permeability, with the membrane flux and Pb^{2+} concentration of the filtrate measured accordingly.

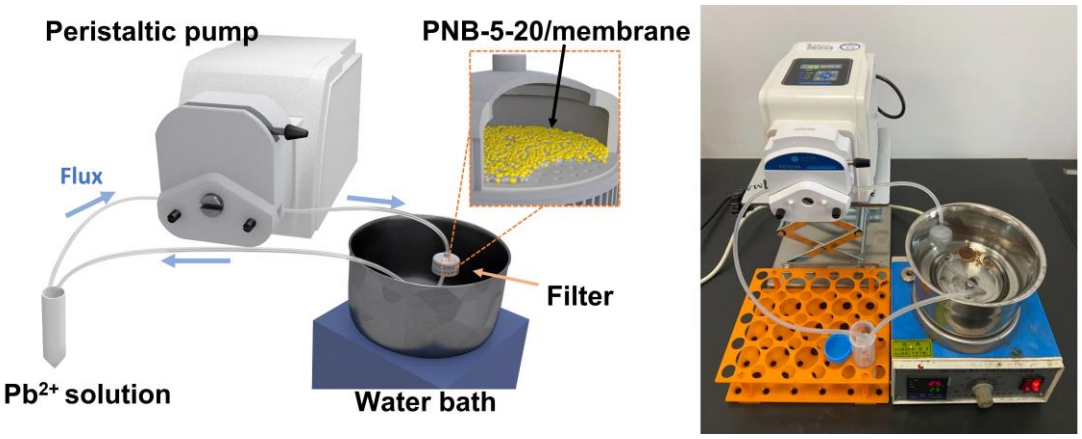

Figure 2. Lab-scale membrane filtration device consisting of a peristaltic pump, a vial holding eluents and a filter unit quipped with PNB-5-20 microgel decorated nylon membrane immersed in a water bath thermostat.

3. Results and discussion

3.1. Synthesis of BCAm monomer and PNB-5-20 microgel

Due to a radius similar to that of Pb^{2+}, the ether ring of B18C6 can selectively chelate with Pb^{2+} to form a "sandwich"-shaped complex with a stoichiometric ratio of crown ether: lead(II) = 2:1 [2]. Hence, B18C6 is promising to be used as a building block to construct a Pb^{2+} recognizer/adsorbent. In order to introduce crown ether groups into the polymer molecular chain and thus the microgel, BCAm monomer was synthesized from B18C6 via nitrification, reduction of the nitro group and then amine acylation. The ^{1}H NMR spectra of the feedstock B18C6, the intermediate N-B18C6, the intermediate A-B18C6, and the product BCAm are shown in Figure 3a.

In the ^{1}H NMR spectra of all the molecules, there is a series of peaks located around 3.7 to 4.2 ppm, which are the characteristic signals of protons in crown ethers. Compared to the ^{1}H NMR spectrum of the feedstock B18C6, two phenyl protons with high chemical shifts of 7.0–8.0 ppm were newly generated in the spectrum of nitrification product N-B18C6. These two signal peaks are attributed to the protons (H^7, H^8) adjacent to the nitro group on the benzene ring. The presence of the nitro group causes a decrease in the electron density of the aromatic ring, therefore

deshielding the protons. This causes the chemical shift of the protons to move to the lower field. Subsequently, the nitro group in N-B18C6 is reduced by hydrazine to amino group in A-B18C6. The electron-donating conjugation of amino group makes the chemical shifts of all the three protons on the benzene ring shift to the higher field (6.0–6.6 ppm). Lastly, in the spectrum of BCAm, three newly generated doublet signals with chemical shifts between 5.5–6.5 ppm are attributed to the alkenyl protons in acrylamide (H^{13}, H^{14}, H^{15}). In addition, a new signal peak at a chemical shift of 7.5–8.0 ppm was attributed to the amide proton (H^{16}). These results indicate that the BCAm was synthesized, that is, polymerizable acryloyl group was successfully introduced to B18C6.

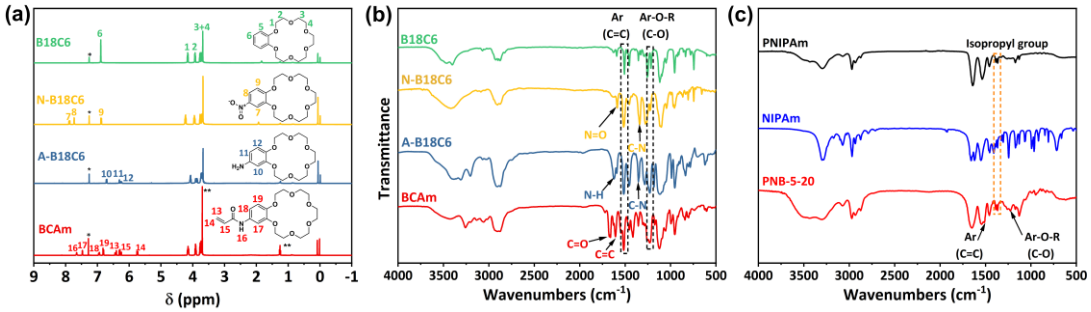

Figure 3. (a) ^{1}H NMR spectra of the B18C6, N-B18C6, A-B18C6, and BCAm (*: $CHCl_3$, **: EtOH); (b) FT-IR spectra of the B18C6, N-B18C6, A-B18C6, and BCAm; (c) FT-IR spectra of PNIPAm and PNB-5-20 microgels.

Moreover, the identities of B18C6, N-B18C6, A-B18C6 and BCAm are confirmed by the FT-IR spectra (Figure 3b). The appearance of N-O symmetric and asymmetric stretching vibration peaks at 1344 cm^{-1} and 1590 cm^{-1}, respectively in the FT-IR spectrum of N-B18C6 compared to that of B18C6 confirmed the successful nitrification. After the reduction, the N-H bending vibration signal at 1617 cm^{-1} is observed in the spectrum of A-B18C6. Lastly, as the amino group was acylated to the acrylamide, the N-H vibration signal diminish, while the signals originating from C=C stretching vibration and C=O stretching vibration are captured at 1607 cm^{-1} and 1670 cm^{-1}, respectively, in the spectrum of BCAm. The IR spectra validated successful synthesis of BCAm with characteristic adsorption identified.

Based on the BCAm synthesized, the PNB-5-20 microgels consisting of NIPAm

units and 18-crown-6 moieties were prepared by precipitation polymerization of BIS, NIPAm and BCAm. ^{1}H NMR spectrum of the PNB-5-20 microgel in D_2O is shown in Figure S1, where the characteristic peaks attributed to BCAm (e.g., the proton in the benzene ring around 6.8–7.0 ppm) and to NIPAm (e.g. the protons on the isopropyl group at 1.0 ppm) segments are well observed. The FT-IR spectra of PNB-5-20 and neat PNIPAm microgels are shown in Figure 3c. The doublet peaks at 1367 cm^{-1} and1388 cm^{-1} in both the spectra of PNIPAm and PNB-5-20 microgels are the characteristic absorption peaks of isopropyl group in the NIPAm unit (orange box in Figure 3c). The characteristic peaks at 1230 cm^{-1} and 1513 cm^{-1} in the IR spectrum of PNB-5-20 are ascribed to C-O asymmetric stretching vibration in Ar-O-R and C=C backbone stretching vibration in benzene ring, respectively [2]. In contrast, the absence of these two peaks in the infrared spectrum of PNIPAm microgel indicates that the crown ether unit has been introduced into the molecular chain of PNB-5-20 microgel, which proves the successful synthesis of PNB-5-20 microgel.

Furthermore, the morphology of PNIPAm and PNB-5-20 microgels in a dried state was observed under SEM and the images are shown in Figure 4. Both PNIPAm and PNB-5-20 microgel particles exhibited well-defined spherical shape with almost mono-dispersed size distribution. The average diameter of PNB-5-20 determined from SEM images is about 300 nm, which is larger than that of the PNIPAm microgel (about 200 nm). This is probably due to that the comonomer BCAm containing acrylamide and crown ether domains is highly hydrophilic at reaction temperature (i.e., 70 °C) in great contrast to the main monomer NIPAm that is known to be hydrophobic at high temperatures. The high hydrophilicity of BCAm favored a good solvation of the microgel during the precipitation polymerization, leading to late precipitation of nucleating particle seeds, lowering of the particle density and thus a larger particle size obtained [52]. In addition, the steric site-blocking effect of benzene ring in BCAm moiety may also result in larger particles of the synthesized microgels [53].

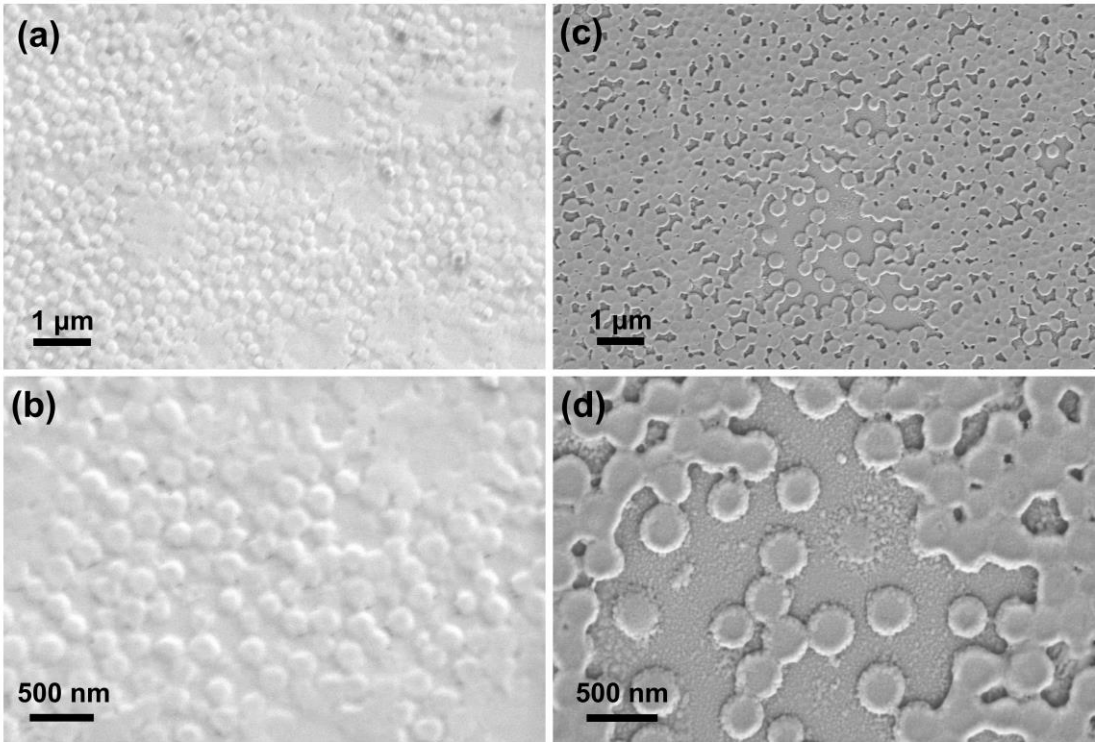

Figure 4. SEM images of (a and b) PNIPAm and (c and d) PNB-5-20 microgels.

3.2. Thermo- and ion-responsiveness of the PNB-5-20 microgel

The temperature- and ion-responsiveness of the PNB-5-20 microgel were investigated by DLS with the hydrodynamic diameter (D_h) of particle measured as a function of temperature at varied Pb^{2+} concentrations (Figure 5). As shown in Figure 5a, in pure water, the PNB-5-20 microgel indicated typical temperature responsiveness similar to PNIPAm with a VPTT around 32.5 °C[54, 55] while the particle size is larger. That is, the PNB-5-20 and PNIPAm microgels shrunk as the temperature increased from 20 °C to 50 °C, with the D_h reduced from 427~~.3~~ nm to 260~~.3~~ nm and from 330 nm to 150 nm, respectively. Note that the particle size measured here is essentially consistent with the SEM characterization, considering the technique difference and the sample state difference. The particle swelling below the VPTT is argued to be a result of the dominant strong hydrogen bonding between the amide groups in PNIPAM chains and water, which dimmish with increased temperature and the hydrophobic interactions between isopropyl groups become dominated whereby water expels from the macromolecules and the particle shrinks.

Since the B18C6 domain was argued to complex Pb^{2+} in an aqueous environment, the temperature dependence of the particle size of PNB-5-20 microgel was expected to show sensitivity to the Pb^{2+}. As presented in Figure 5, a low Pb^{2+} concentration (0.05 mM) subtly affects the particle size of PNB-5-20 microgels, while a concentration as high as 0.5 mM can increase the particle size in swollen state from 427~~.3~~ nm to ~500 nm with the VPTT lightly shifted by ~ 1 °C. A further increase of the Pb^{2+} concentration to 5 mM enormously enlarged the particle size of PNB-5-20 microgel in swollen state to ~ 650 nm and the VPTT was also significantly shifted from 33 °C to 43 °C but the particle was finally collapsed to a similar size ~ 330 nm at high temperatures (> 50 °C). This indicates that the PNB-5-20 microgel has good dual responsiveness towards both temperature and Pb^{2+}, with the temperature-responsiveness readily regulated by the Pb^{2+} concentration.

Moreover, to evaluate the responsiveness selectivity of PNB-5-20 microgels to Pb^{2+}, temperature dependence of the particle size in the presence of different ions was investigated at the same ion concentration (i.e., 5 mM). As shown in Figure 5b, in contrast to the stable dispersion with particles largely swollen in 5 mM Pb^{2+} solution, in Na^+, K^+ and Cs^+ solutions the PNB-5-20 microgels were found to start to agglomerate above 35 °C, 32 °C, and 30 °C, respectively. The agglomerations are due to the electrolyte screening of the electrical double-layer repulsion of particle surface charge, which dominate the colloidal stability when the microgel begins shrinking. The difference on the effects between Pb^{2+} and the other metal ions, could be ascribed to the comparable cavity size of B18C6 (3.41 Å)[56] and hydrodynamic radius of Pb^{2+} (4.01 Å)[57] rather than those of tested alkali ions (Na^+, K^+, Cs^+, < 2.5 Å)[58]. This indicates the high selectivity of the PNB-5-20 microgel on recognizing Pb^{2+}.

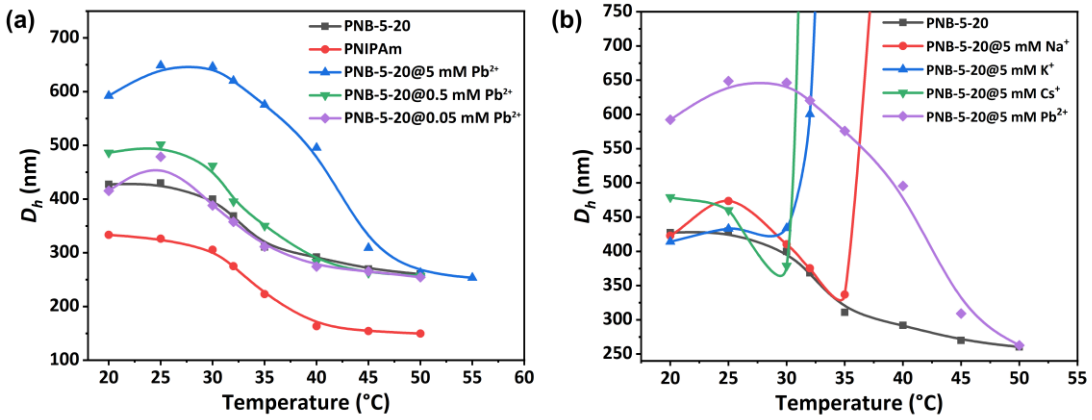

Figure 5. (a) Variation of the particle size of PNB-5-20 microgel with temperature measured in pure water and in solutions with different Pb^{2+} concentrations; (b) Variation of the particle size of PNB-5-20 microgel with temperature measured in different metal ion solutions with the same ion concentration (5 mM).

3.3. Lead (II) adsorption

3.3.1. Isothermal adsorption

Isothermal adsorption experiments were performed to determine the adsorption capacity of PNB-5-20 microgels for Pb^{2+}. The adsorption quantities of Pb^{2+} by PNB-5-20 microgel (q, mg adsorbate/g adsorbent) was plotted against the equilibrium Pb^{2+} concentration in solution (C_e, ppm) after adsorption (Figure 6a). The isothermal adsorption by PNIPAm microgel was also investigated as reference based on the same procedure. To evaluate the adsorption capability of the two microgels, the adsorption data are fitted by the Langmuir and Freundlich models. The Langmuir model assumes homogeneous monolayer adsorption, while the Freundlich model describes non-homogeneous multilayer adsorption.[59] The Langmuir and Freundlich adsorption models can be expressed by equations (3) and (4), respectively:

$$q = \frac{bq_m C_e}{1+bC_e} \quad (3)$$

$$q = K_F C_e^n \quad (4)$$

where b is Langmuir's constant (L mg^{-1}) related to the affinity coefficient of the binding site, q_m is the maximum adsorption capacity for Pb^{2+}; K_F is the Freundlich

462 adsorption coefficient, and *n* is the strength of adsorption.

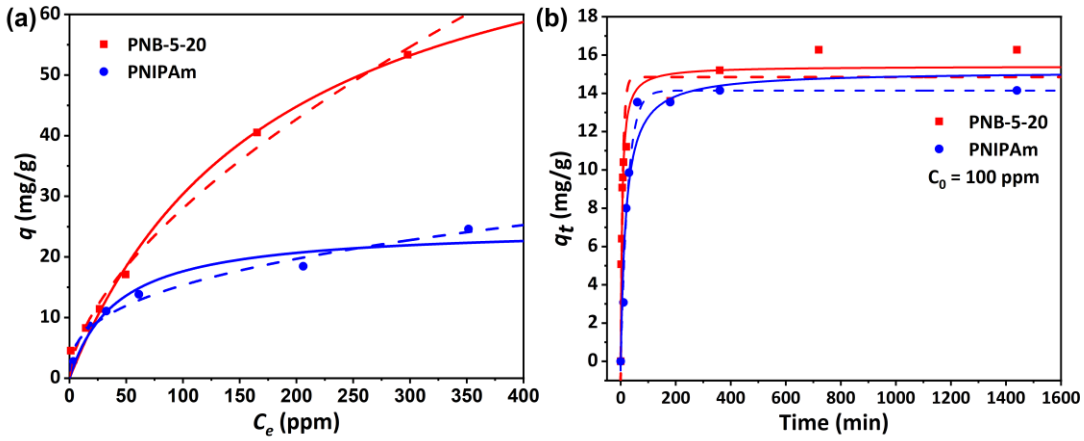

463

464 Figure 6. (a) Pb^{2+} adsorption isotherms for PNB-5-20 and PNIPAm microgels. The solid and
465 dashed lines are obtained by fitting the isotherm with Langmuir and Freundlich model,
466 respectively; (b) adsorption kinetics of PNB-5-20 and PNIPAm microgels at C_0 = 100 ppm. The
467 solid and dashed lines are the fitting results according to pseudo- second-order and
468 pseudo-first-order kinetic models, respectively.

469

470 Table 2 lists the fitted parameters of Langmuir and Freundlich models. The
471 adsorption data of PNB-5-20 microgel can be well fitted by Langmuir and Freundlich
472 isotherms with correlation coefficients (R^2) as high as 0.989 and 0.991, respectively.
473 The adsorption capacity of the PNB-5-20 microgel was estimated to be 85.4 mg/g
474 from the fitted Langmuir model. In contrast, although the neat PNIPAm microgel
475 show affinity to Pb^{2+}, its adsorption capacity (q_m = 25.0 mg/g) is significantly smaller
476 than that of PNB-5-20, indicating the remarkable contribution of 18-crown-6 ether
477 moieties to Pb^{2+} adsorption. The correlation coefficients of the Langmuir isotherms
478 (PNB-5-20, R^2 = 0.989; PNIPAm, R^2 = 0.953) were slightly smaller than those of the
479 Freundlich isotherms (PNB-5-20, R^2 = 0.991; PNIPAm, R^2 = 0.975), suggesting that
480 the Freundlich model is also suitable to describe the adsorption of Pb^{2+} on PNB-5-20
481 and PNIPAm microgels. This implies that the adsorption sites may be not uniformly
482 distributed on the surface of the microgels, but a certain number of adsorption sites
483 are also distributed in the interior of the microgels and the adsorption behaviors of
484 different sites are expected to interfere with each other. The phenomenon could be

attributed to the relatively compact core and fuzzy corona structure of the microgels [60] synthesized from precipitation polymerization of NIPAm.

Table 2. Fitted parameters in the Langmuir and Freundlich isotherm models for Pb^{2+} adsorption.

Sample	Langmuir model			Freundlich model		
	q_m (mg/g)	b (L/mg)	R^2	K_F ($mg^{1-n} \cdot L^n/g$)	n	R^2
PNB-5-20	85.4±10.2	0.006±0.001	0.989	1.704±0.382	0.608±0.042	0.991
PNIPAm	25.0±2.1	0.024±0.007	0.953	2.928±0.543	0.360±0.036	0.975

3.3.2. Adsorption kinetics

In order to further evaluate the Pb^{2+} adsorption rate by PNB-5-20 microgels, the adsorption kinetics were investigated at an initial Pb^{2+} concentration of 100 ppm, and the results are shown in Figure 6b. The classical pseudo-first-order and pseudo-second-order kinetic models describing the ion adsorption process were used to fit the experimental data. The pseudo-first-order and pseudo-second-order kinetics were expressed by the equations (5) and (6):

$$q_t = q_e(1 - e^{-k_1 t}) \quad (5)$$

$$q_t = \frac{k_2 q_e^2 t}{1 + k_2 q_e t} \quad (6)$$

where q_t and q_e are the amount of Pb^{2+} adsorbed (mg g^{-1}) at time t and when adsorption equilibrium is reached, respectively; k_1 and k_2 are the primary and secondary rate constants, respectively. The fitted curves are superimposed with experimental data in Figure 6b with parameters listed in Table 3.

Table 3. Fitting parameters of pseudo-second-order and pseudo-first-order models for Pb^{2+} adsorption by PNB-5-20 and PNIPAm microgels.

Sample	Pseudo-second-order			Pseudo-first-order		
	k_2 (g mg^{-1} min^{-1})	q_e (mg g^{-1})	R^2	k_1 (min^{-1})	q_e (mg g^{-1})	R^2
PNB-5-20	0.0131±0.0018	15.41±0.42	0.976	0.133±0.019	14.85±0.64	0.937
PNIPAm	0.0035±0.0010	15.14±0.86	0.953	0.039±0.004	14.14±0.41	0.985

Based on the fitted results (Table 3), it can be seen that the adsorption kinetics of neat PNIPAm microgel conformed to the pseudo-first-order model (R^2 = 0.985) whereas PNB-5-20 conformed better to the pseudo-second-order model (R^2 = 0.976) than the first-second-order model (R^2 = 0.937). This might suggest that the adsorption kinetic behavior of PNB-5-20 microgel for Pb^{2+} is chemisorption rather than physisorption [59]. More exactly, the adsorption rate of PNIPAm to Pb^{2+} is limited by the diffusion process due to the few number of active site while the adsorption rate of PNB-5-20 is dominated by the sorption onto active sites due to its abundance [61]. This can be verified by the experimental observations. For instance, the PNIPAm microgel reached adsorption equilibrium in about 50 min at an initial concentration of 100 ppm of Pb^{2+}. The adsorption rate constant based on the pseudo-first-order modeling of the PNIPAm microgel was fitted to be 0.039 min^{-1}. In contrast, the adsorption rate of Pb^{2+} by the PNB-5-20 microgel was quite fast, reaching the adsorption equilibrium in only about 10 min. The first-order rate constant of PNB-5-20 (0.133 min^{-1}) as well as equilibrium adsorption (q_e = 14.85 mg/g) was larger than that of PNIPAm microgel. The results illustrate that the incorporation of the B18C6 domain into the microgels not only increase the adsorption sites but also accelerates the adsorption, therefore enabling its application in membrane purification which required fast adsorption in light of the high fluxes.

3.3.3. pH, temperature and competing ion effects

Polluted water in the natural environment or industrial effluents may have various pH and temperatures, and these parameters may affect the adsorption capability of the PNB-5-20 microgel. Therefore, it is essential to test the adsorption ability of PNB-5-20 microgel under different pH and temperatures (Figure 7a&b) to evaluate if the responsive PNB-5-20 adsorbent can be utilized in complicated aqueous systems.

For the effect of pH, the adsorption experiments were carried out at C_0 = 100 ppm and pH ranging from 2 to 10, the adsorption quantities q is plotted against the pH. As shown in Figure 7a, the adsorption capacity of PNB-5-20 microgel significantly declines with decreased pH from 10 to 2. It could be explained by the competition for adsorption sites, i.e., crown ether, by high concentrations of H^+ in the low pH solutions, which undermines the Pb^{2+} adsorption. In particular, the declining effect is significant as the pH decreased from 6 to 2, but subtle in the range of pH 6–10, wherein the PNB-5-20 microgel maintain a good adsorption performance.

On the other hand, the effect of temperature on the adsorption performance was evaluated by testing the Pb^{2+} removal (R, %) at C_0 = 20 ppm in the temperature range of 25–40 °C. R was calculated by Eq. (7):

$$R = \frac{C_0 - C_e}{C_0} \times 100\% \quad (7)$$

where C_0 and C_e (mg L^{-1}) are the initial concentration of Pb^{2+} and the concentration at adsorption equilibrium, respectively. As shown in Figure 7b, although the removal efficiency of PNB-5-20 microgel decreased with increasing temperature, the decrease was minor and there was still a considerable Pb^{2+} removal obtained at 40 °C, confirming a robust adsorption capability across the VPTT of the microgel, which suggests the collapse of microgel does not interfere the adsorption.

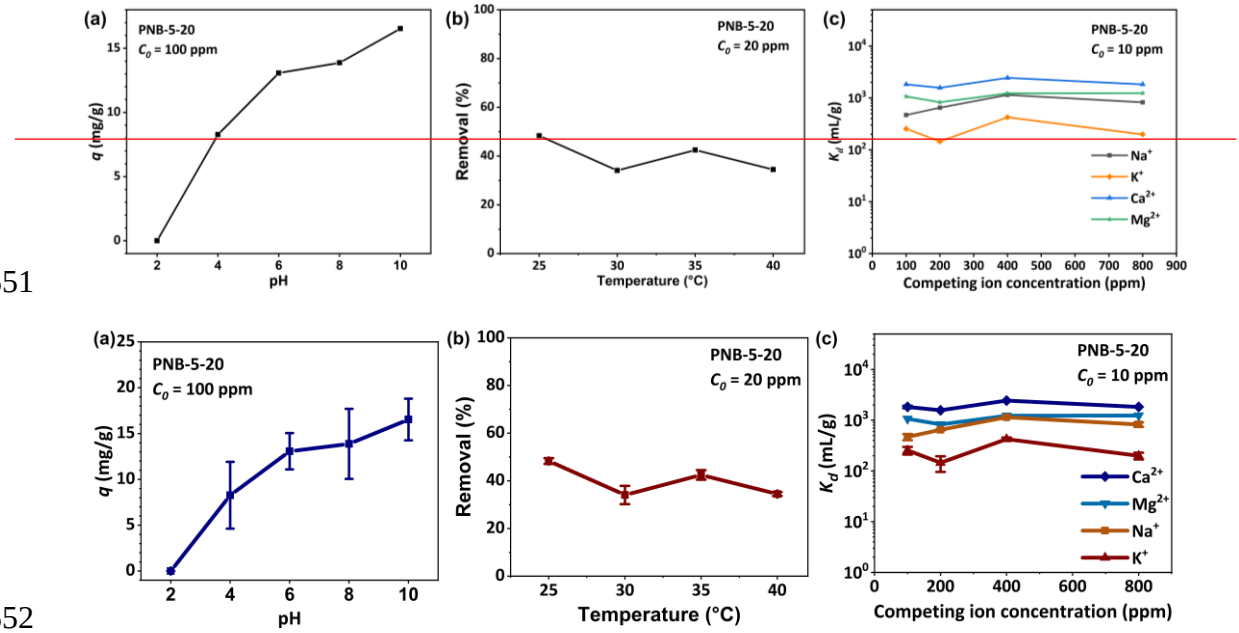

Figure 7. Effect of pH, temperature and competing ions on adsorption of PNB-5-20 microgel. (a) Pb^{2+} adsorption capacity versus pH at C_0 = 100 ppm; (b) Pb^{2+} removal versus temperature at C_0 = 20 ppm; (c) distribution coefficient K_d versus competing ion concentration of the microgel in adsorbing Pb^{2+} (C_0 = 10 ppm) in aqueous solutions containing Na^+, K^+, Ca^{2+}, or Mg^{2+}, respectively.

Other inorganic ions in water may affect the adsorption process of target ions [62]. Among them, Na^+, K^+, Ca^{2+} and Mg^{2+} are the most common competing ions for Pb^{2+} in polluted water. In order to determine the adsorption selectivity of PNB-5-20 microgels to Pb^{2+}, PNB-5-20 microgels were dispersed in Pb^{2+} solutions (C_0 = 10 ppm) containing different concentrations of Na^+, K^+, Ca^{2+}, or Mg^{2+} (100–800 ppm), and the concentration of adsorbed Pb^{2+} was detected by ICP-OES. The Pb^{2+} selectivity was evaluated by the distribution coefficient K_d:

$$K_d = \frac{C_0 - C_e}{C_e}\frac{V}{m} \quad (8)$$

where C_0 and C_e are the initial and equilibrium concentrations of Pb^{2+}, V is the volume of the solution (mL), m is the mass of the adsorbent (g).[63, 64]

A larger value of K_d indicates that the corresponding competing ions interfere less with the adsorption of the target ion, i.e., the selectivity of the adsorbent to the target ion is better. Conversely, the smaller the value of K_d, the relatively poor

572 selectivity of the adsorbent to the target ion.

573 The K_d in the presence of different competing ions, Na^+, K^+, Ca^{2+} or Mg^{2+}, with
574 varied concentrations is illustrated in Figure 7c. It can be seen that the PNB-5-20
575 microgel has a good selectivity to Pb^{2+} with a K_d around 10^3 mL/g regardless of the
576 type of competing ions, and the high concentration (e.g., 800 ppm) of competing ions
577 barely undermines the selectivity. Among the ions, the interference of Ca^{2+} with the
578 adsorption of Pb^{2+} by the PNB-5-20 microgel is the least, while the competition for
579 adsorption sites by K^+ is evident. This is due to the fact that the ionic diameter of K^+
580 matches the diameter of the crown ether cavity in B18C6, which could form stable
581 complexes similar to Pb^{2+} [53, 65]. Nevertheless, the PNB-5-20 microgel exhibits better
582 selectivity to Pb^{2+} rather than other ions including K^+ judging from K_d. This suggests
583 that PNB microgels can selectively recover Pb^{2+} in real aqueous environments for
584 practical applications.

585 Lastly, the adsorption capability of the PNB-5-20 microgel is compared with
586 reported materials used to construct adsorptive membranes (Table 4). It can be seen
587 that among the adsorbents, the microgel has decent adsorption capacity (85.4 mg/g)
588 with the fastest adsorption rate in term of low equilibrium time (10 min). The fast
589 adsorption is ascribed to the hydrophilicity of microgel at the adsorption temperature,
590 where the Pb^{2+} can diffuse rapidly into the water-swollen microgel and be captured by
591 the 18-crown-6 moieties. In light of the good kinetic responsiveness to Pb^{2+}, although
592 not having the highest adsorption capacity, PNB-5-20 is an excellent responsive
593 material to construct smart membrane, allowing rapid permeation of clean water while
594 intercepting Pb^{2+} discriminately and quickly without sacrificing adsorption capability.
595 Moreover, the Pb^{2+} removal efficiency and response amplitude of the smart membrane
596 can be readily regulated by changing the amount of the PNB-5-20 used in the
597 preparation to cope with polluted water containing different concentrations of Pb^{2+}.
598

599 Table 4 Comparison of adsorption performance for Pb^{2+} removal by different
600 adsorptive membranes.

Membranes	Equilibrium (min)	q_{max} (mg/g)	Reference
Polysulfone/hydrous ferric oxide ultrafiltration mixed matrix membrane	720	13.2	[40]
chitosan/cellulose acetate blend membrane with dithizone	100	25.0	[66]
Ferrihydrite nanoparticles/polyethersulfone composite membrane	360	64.8	[41]
chitosan/polyacrylonitrile	30	20.1	[67]
polyethersulfone /hydrous manganese dioxide mixed matrix membranes	600	204.1	[42]
zirconium phosphate modified polyvinyl alcohol- Polyvinylidene fluoride membrane	300	121.2	[43]
polyacrylonitrile/hydroxyapatite composite nanofibrous membranes	300	111.9	[68]
Hybrid membrane of cellulose acetate with zinc oxide	Not reported	15.6	[69]
nanofibrillated cellulose/carbon nanotubes/Didymo membrane	Not reported	129.0	[39]
PNB-5-20 microgel loaded on Nylon membrane	10	85.4	This study

601

3.3.4. Adsorption mechanism

To reveal the adsorption mechanism of PNB-5-20 to Pb^{2+}, the elemental composition as well as their chemical environments were studied by XPS (Figure 8). From the broad survey XPS spectrum (Figure 8a), it is clear that a Pb 4f signal appeared in the spectrum of PNB-5-20 after adsorption experiment (PBN-5-20-Pb^{2+}), indicating the enrichment of Pb^{2+} in the microgel. In particular, the high-resolution O 1s spectra marked that the binding energy of crown ether oxygens at ~ 540 eV and ~ 536 eV (PNB-5-20) significantly shift to ~538 eV and 535 eV (PNB-5-20-Pb^{2+}), respectively, after the adsorption of Pb^{2+}. The binding energy alteration suggests that the adsorption of Pb^{2+} is accomplished via the chelation of Pb^{2+} by crown ether thereby the O 1s electron became easy to escape, which is also observed in XPS spectra of other Pb^{2+} adsorbents reported in literature [17, 70-72]. On the other hand, the high-resolution Pb 4f spectrum (Figure 8b) revealed that the all Pb atoms are present as Pb^{2+} in the adsorbent, confirming the single adsorption mechanism. The XPS spectra demonstrated the specific complexation between Pb^{2+} and the B18C6 moieties contributes to the high adsorption capability and selectivity of the PNB-5-20 microgel.

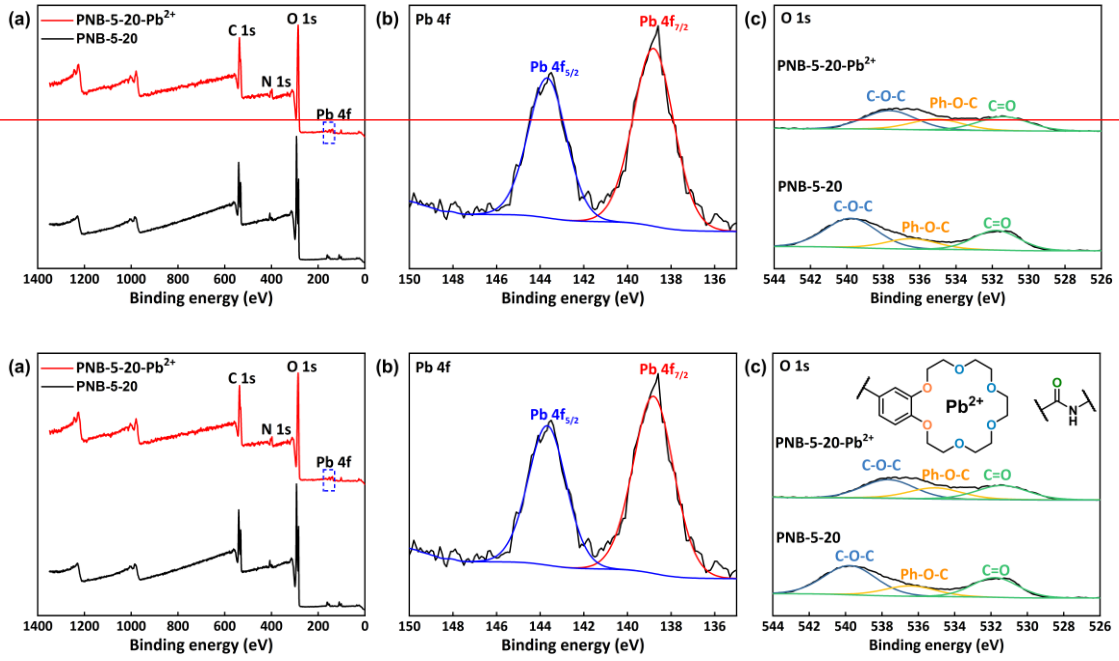

Figure 8. XPS spectra of PNB-5-20 microgel before and after the adsorption of Pb^{2+} (C_0 = 59.4 ppm): (a) Broad survey XPS spectrum and high-resolution spectrums of (b) Pb 4f, (c) O 1s photoelectron.

3.3.5. Membrane filtration

Ultimately, a smart membrane filtration device with a Pb^{2+}- and temperature-responsive water gating system was fabricated (Figure 2), in which a Nylon filter membrane (pore size 0.45 μm, diameter 25 mm) was loaded with PNB-5-20 microgels under vacuum and then placed into a PP filter unit. To evaluate the dual responsiveness of the water gating system of the functionalized membrane, model filtration experiment was performed to monitor the liquid permeability change of the membrane in response to the presence of Pb^{2+} and to the temperature alternation. At the same time, the change of Pb^{2+} concentration in the liquid was monitored to check the purification efficiency. In particular, DI water was first circulated through the functionalized membrane at 25 °C. Subsequently, at t = 10 min, a given amount of Pb^{2+} solution was added into the reservoir to obtain a Pb^{2+} concentration of 0.5 mM in the eluent and the permeability was continuously tested to check the interception of the Pb^{2+}-polluted water by the functionalized membrane. The Pb^{2+} concentration in the circulating effluent was plotted in Figure 9. Lastly, at t = 30 min, the temperature of the water bath was adjusted to 40 °C to study the responsiveness of the membrane to temperature.

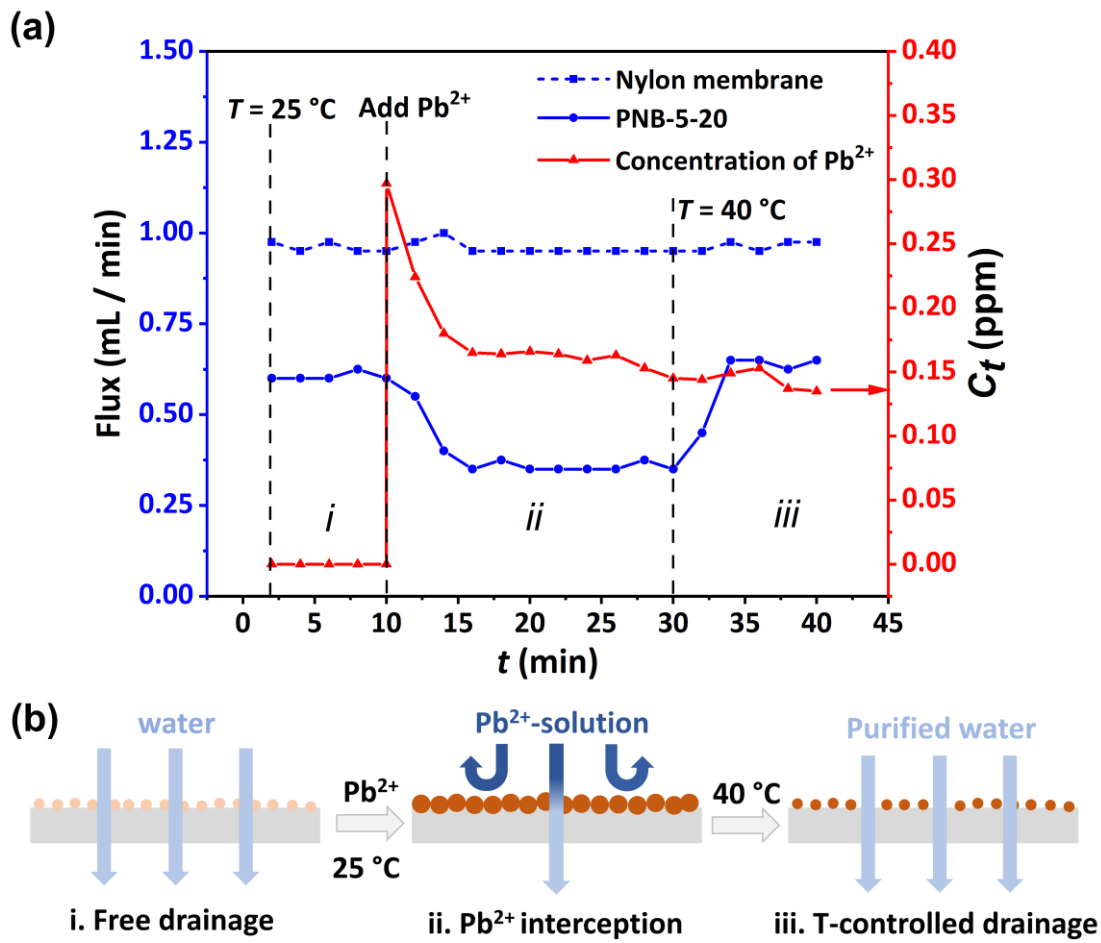

Figure 9. (a) Membrane flux and Pb^{2+} concentration versus time in a continuous filtration experiment at 25 °C with Pb^{2+} added at t =10 min and temperature raised to 40 °C at t = 30 min. (b) Illustration of the alteration in membrane structures and therefore the flux due to the responsiveness of the microgel to Pb^{2+} and temperatures.

As shown in Figure 9, with PNB-5-20 microgels loaded on the Nylon filtration membrane, the membrane permeability of DI water was reduced, from ~ 1.0 mL/min in the unmodified Nylon membrane to ~ 0.6 mL/min in the functionalized membrane. This indicates the PNB-5-20 microgels were immobilized in the membrane pores with the water permeation partially resisted, acting as water gates in the pores. When Pb^{2+} was recognized at t = 10 min (C_0 = 59.4 ppm), the liquid flux started to gradually decrease to about 0.34 mL/min in ~ 6 mins and at the same time the Pb^{2+} concentration in the circulating effluent declined to 33 ppm. Undoubtedly, this is ascribed to the swelling of the PNB-5-20 microgels when recognizing and adsorbing the Pb^{2+}, making the water gate in membrane pores switch from “open” to “closed”

state with the highly swollen microgels jamming the pores of membrane, rejecting the water from permeating across the membrane. The retention of Pb^{2+} polluted water allows it to be purified via the efficient adsorption of Pb^{2+} by microgels in the functionalized membrane. Obviously, the Pb^{2+} responsiveness of PNB-5-20 microgel, that is, significant swelling with Pb^{2+} (see Fig.5a), plays an essential role in spontaneously regulating the filtration water gate, which is useful not only for a selective filtration and purification of polluted water but also for monitoring water contamination as a potential sensor.

Lastly, once the water was purified, the water gate can be readily regulated to "re-open" by raising the membrane temperature above the VPTT of the PNB-5-20-Pb^{2+} microgels (e.g., 40 °C) whereby the microgels can shrink into dense particles with reduced size (Figure 5). As shown in Figure 9, upon heating to 40 °C at t = 30 min, the water flux was observed to recover to about 0.65 mL/min in ~ 4 mins as a result of microgel collapse. Undoubtedly, the change of water permeability with temperature indirectly verifies the tunability of the microgel-loaded membrane pore size as the microgels attached inside the pores and/or covered on the membranes can collapse upon heating (Fig.5) whereby pore spaces are enlarged for permeation. Meanwhile, the Pb^{2+} concentration in the circulating effluents remained at a low level ~ 27 ppm, indicating no release of the adsorbed Pb^{2+} from microgel into liquid during the heat-induced particle shrinking process. This suggests the stable chelation of Pb^{2+} by the crown ether-functionalized microgel in contrast to the reported application of B18C6-functionalized microgels in Li^{+} enrichment [73] where adsorbed Li^{+} escaped from the microgel in response to elevated temperatures.

In summary, the dual responsive PNB-5-20 microgel enables development of a smart filtration membrane to regulate the water permeability in response to the presence of Pb^{2+} and temperature change, allowing interception of polluted water spontaneously to be purified synchronously before being discharged to the environment at willing by heating the membrane. This is in great contrast to the

688 negligible variation of water flux in neat nylon 6 membrane after being subjected to
689 the identical treatments (i.e., presence of Pb^{2+} and change of temperature) (Figure 9).
690 Comparing with the rarely reported Pb^{2+}-responsive devices in literature [74, 75], the
691 smart membrane established herein has great advantages of facile preparation and
692 large response amplitude in the transmembrane flux. The microgels were loaded on
693 the membrane without need of chemical linkage thereby allowing flexibility in
694 fabricating the composite membrane and work-up after filtration. Moreover, the smart
695 membrane prepared also exhibit an obvious decrease in the flux (0.65 to 0.35 mL/min)
696 when recognizing the Pb^{2+} comparing to the literature (0.33 to 0.25 mL/min) [75],
697 suggesting a better responsiveness to Pb^{2+} which would favor its application in
698 intercepting and sufficiently purifying Pb^{2+}contaminated water.

699 After the continuous filtration experiment, the functionalized membrane was
700 removed from the PP filter unit and dried in the air before being analyzed by SEM
701 and EDX to verify the Pb^{2+} adsorption on the membrane. The neat nylon6 membrane
702 and the clean functionalized membrane (PNB-5-20 loaded) were also measured as
703 control samples and the results are shown in Figure 10 and Figure S2. As shown in
704 Figure 10a, the nylon6 membrane without microgels is a distinctly porous material
705 having numerous pores with various sizes that allow water to pass through
706 unimpededly under given experimental conditions. After loading with PNB-5-20
707 microgels, most of the pores on the surface and inside the nylon membrane were
708 occupied by the microgels, as confirmed by the reduced number of pores especially
709 the disappearance of small pores observed in Figure 10b. The reduction in number of
710 pores (c.a. 6,400 to c.a. 4,100 in the view) and the roughness is demonstrated by
711 analyzing the SEM images through ImageJ software (Figure S3 and S4) based on
712 binary images, ~~and by~~ which is further confirmed by the reduced membrane flux
713 shown in Figure 9 in comparison to that of neat nylon membrane. Higher resolution
714 SEM images of PNB-5-20 microgels loaded membrane are given in Figure S2.

715 After the continuous filtration under pressure experiencing water gate “closed”

and "re-open" with Pb^{2+} adsorbed and membrane heated, part of the microgels on the membrane surface were driven into the membrane interior by the transmembrane pressure, as shown in Figure 10c. From the EDX elemental maps (Figure 10d), it can be seen that the surface of the membrane as well as the pores show a strong signal of elemental Pb. This indicates that the PNB-5-20 microgels accumulated on the surface of the nylon membrane and attached in the pores of the nylon membrane successfully adsorbed Pb^{2+}.

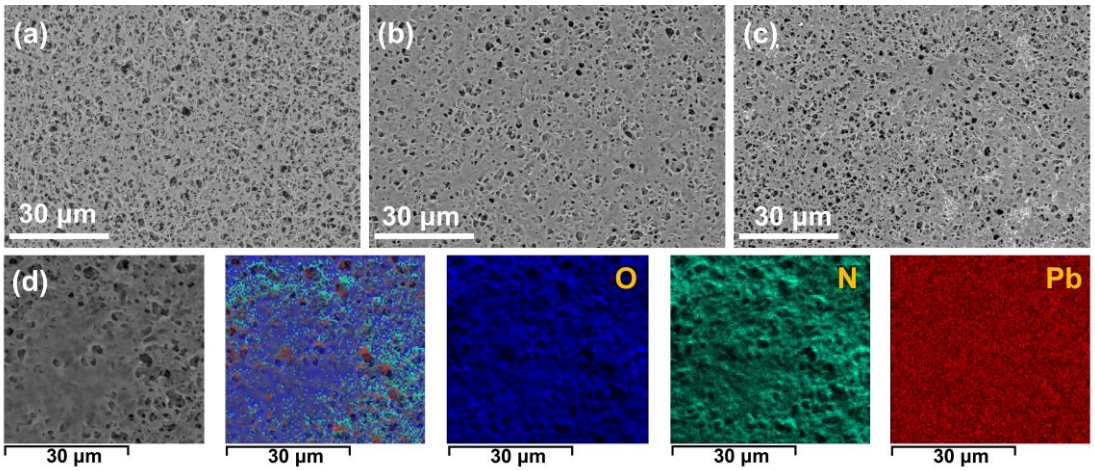

Figure 10. SEM images of (a) nylon membrane, PNB-5-20 microgel loaded membranes (b) before and (c) after subjected to Pb^{2+}-responsive filtration test. (d) The distribution of O, N, and Pb in the EDX elemental maps of membranes with adsorbed Pb^{2+} are shown in blue, cyan, and red, respectively.

Lastly, the cost of the PNB-5-20 microgel and microgel-functionalized membrane is calculated (see Supporting Information for details) to evaluate its feasibility in practical remediation of Pb^{2+}polluted waste water. Based on the prices of feedstocks as well as their feed ratios and the product yields in synthesis, the cost of PNB-5-20 microgel is estimated to be ~$7/g, while 1 g PNB-5-20 microgel can functionalize about 0.41 m^2 membrane, able to remedy about 2800 L real waste water (C_0 = 0.03 ppm) from Pb^{2+} polluted areas.[76] The calculations indicate that our microgel-functionalized membrane is affordable for inhabitants in polluted areas to be used in a household water purifier. Moreover, as the microgel synthesis is possible to be scaled up, the cost of the microgel-functionalized membrane could be further

lowered with large-scale production. Anyhow, microgel-functionalized membrane is promising in practical water treatment considering its low price and good adsorption capability.

4. Conclusions

In this work, inspired from oleander roots, a smart microgel-loaded filtration membrane with a thermo- and Pb^{2+}- dual responsive water gating system has been developed for effective Pb^{2+} separation by loading thermo- and Pb^{2+} responsive microgels PNB-5-20, which is synthesized from NIPAm and benzo-18-crown-6, on a commercial nylon membrane. ~~Firstly, a monodisperse thermo- and Pb^{2+}- dual responsive microgel, poly(*N*-isopropylacrylamido-*co*-acrylamido-benzo-18-crown-6) (PNB-5-20), with a well-defined structure bearing crown ether moieties was prepared by precipitation copolymerization of NIPAm and BCAm, which was synthesized from sequential nitrification, reduction of nitro group and acylation of B18C6.~~ The PNB-5-20 exhibits a pronounced thermo-responsiveness, having the particle size (D_h) reduced from 427~~.3~~ nm to 260~~.3~~ nm with a VPTT around 33 °C~~. Moreover, the microgel shows~~, and a striking responsiveness selectively to Pb^{2+} ~~due to the complexation of Pb^{2+} with the B18C6 domains, which facilitated the~~ as evidenced by the swelling of microgel with a significant increase in D_h to ~ 650 nm at 20 °C and in the VPTT to 43 °C. Furthermore, the PNB-5-20 can adsorb Pb^{2+} with a high capacity (85.4 mg/g)~~. The adsorption follows pseudo-second-order kinetic with a rate constant of 0.133 min^{-1}~~, having the adsorption equilibrium reached in less than 10 minutes. Also, the microgel exhibits excellent sorption selectivity to Pb^{2+} in the presence of Na^+, K^+ and Cs^+, and the adsorption ~~to Pb^{2+}~~ remains robust in varied temperatures ~~albeit being suppressed in low pH environment~~. ~~Lastly, the smart filtration membrane was developed by loading PNB-5-20 microgels on a Nylon membrane under vacuum, whereby~~ By loaded with PNB-5-20, the porous membrane was ~~pores were~~ endowed

with responsiveness to temperature and Pb^{2+} as a smart water gating system. The functionalized membrane can recognize Pb^{2+} and retard the permeation of Pb^{2+} solution with the pores jamming by swollen microgels adsorbing Pb^{2+}, while by raising temperature the jammed swollen microgels reversibly collapse resulting in discharge of the purified water. The microgel-functionalized filtration membrane combines detection, adsorption of Pb^{2+} and regulatable water drainage in a single device, exhibiting great potential in practical Pb^{2+} remediation with advantages of simple operation, low energy consumption and high efficiency.

Acknowledgements

This research was financially supported by the National Natural Science Foundation of China (22172028), and the Natural Science Foundation of Fujian Province of China (2020J01145 and 2022J05041). H. Z. acknowledges the Award Program of Fujian Minjiang Scholar Professorship (2018) and D. H. acknowledges the "100 Foreign Experts" of Fujian Province of China (2023) for the support.

ASSOCIATED CONTENT

Supporting Information

The Supporting Information is available free of charge at XXXX

^{1}H NMR spectrum of the microgel, top view and cross-sectional SEM image of microgel-functionalized membrane, and techno-economic evaluation of the product. (PDF)

AUTHOR INFORMATION

Corresponding Authors

*E-mail: huagui.zhang@fjnu.edu.cn (H. Zhang)

Notes

The authors declare no competing interest.

References

(1) Wang, S.; Razanajatovo, M. R.; Du, X.; Wan, S.; He, X.; Peng, Q.; Zhang, Q. Recent advances on decomplexation mechanisms of heavy metal complexes in persulfate-based advanced oxidation processes. *Chin. Chem. Lett.* **2024**, *35* (6), 109140.

(2) Wang, Y.; Liu, Z.; Luo, F.; Peng, H.-Y.; Zhang, S.-G.; Xie, R.; Ju, X.-J.; Wang, W.; Faraj, Y.; Chu, L.-Y. A novel smart membrane with ion-recognizable nanogels as gates on interconnected pores for simple and rapid detection of trace lead(II) ions in water. *J. Membr. Sci.* **2019**, *575*, 28-37.

(3) Youness, F.; Jaafar, A.; Tehrani, A.; Bilbeisi, R. A. Functionalised electrospun membranes (TETA-PVC) for the removal of lead(ii) from water. *RSC Adv.* **2022**, *12* (38), 24607-24613.

(4) Zheng, Z.; Liu, J.; Zhang, M.; Li, H.; Pan, J. A crescent-shaped imprinted microgel adsorbent with near-infrared light-responsive performance for selective adsorption of Lead(II). *Sep. Purif. Technol.* **2024**, *328*, 124963.

(5) Karim, M. R.; Aijaz, M. O.; Alharth, N. H.; Alharbi, H. F.; Al-Mubaddel, F. S.; Awual, M. R. Composite nanofibers membranes of poly(vinyl alcohol)/chitosan for selective lead(II) and cadmium(II) ions removal from wastewater. *Ecotoxicol. Environ. Saf.* **2019**, *169*, 479-486.

(6) Chen, D.; Shen, W.; Wu, S.; Chen, C.; Luo, X.; Guo, L. Ion exchange induced removal of Pb(II) by MOF-derived magnetic inorganic sorbents. *Nanoscale* **2016**, *8* (13), 7172-7179.

(7) Yetilmezsoy, K.; Demirel, S. Artificial neural network (ANN) approach for modeling of Pb(II) adsorption from aqueous solution by Antep pistachio (Pistacia Vera L.) shells. *J. Hazard. Mater.* **2008**, *153* (3), 1288-1300.

(8) Ren, Y.; Yan, N.; Feng, J.; Ma, J.; Wen, Q.; Li, N.; Dong, Q. Adsorption mechanism of copper and lead ions onto graphene nanosheet/δ-MnO_2. *Mater. Chem. Phys.* **2012**, *136* (2), 538-544.

(9) Rasheed, H. M.; Rauf, A.; Arif, M.; Mohyuddin, A.; Javid, M.; Nadeem, S.; Yousuf, A.; Irfan, M.; Haroon, S. M.; Raza, H.; et al. Selective Removal of Lead (II) Ions from Wastewater with Fabricated ZnO-PVA Membrane. *JOM* **2023**, *75* (12), 5310-5320.

(10) Aroua, M. K.; Leong, S. P. P.; Teo, L. Y.; Yin, C. Y.; Daud, W. M. A. W. Real-time determination of kinetics of adsorption of lead(II) onto palm shell-based activated carbon using ion selective electrode. *Bioresour. Technol.* **2008**, *99* (13), 5786-5792.

(11) Jang, S. H.; Min, B. G.; Jeong, Y. G.; Lyoo, W. S.; Lee, S. C. Removal of lead ions in aqueous solution by hydroxyapatite/polyurethane composite foams. *J. Hazard. Mater.* **2008**, *152* (3), 1285-1292.

(12) Ju, X.-J.; Zhang, S.-B.; Zhou, M.-Y.; Xie, R.; Yang, L.; Chu, L.-Y. Novel heavy-metal adsorption material: ion-recognition P(NIPAM-co-BCAm) hydrogels for removal of lead(II) ions. *J. Hazard. Mater.* **2009**, *167* (1), 114-118.

(13) Briffa, J.; Sinagra, E.; Blundell, R. Heavy metal pollution in the environment and their toxicological effects on humans. *Heliyon* **2020**, *6* (9), e04691.

(14) Shahat, A.; Hassan, H. M. A.; Azzazy, H. M. E.; El-Sharkawy, E. A.; Abdou, H. M.; Awual, M. R. Novel hierarchical composite adsorbent for selective lead(II) ions capturing from wastewater samples. *Chem. Eng. J.* **2018**, *332*, 377-386.

(15) Wang, Y.; Liu, Z.; Peng, H. Y.; He, F.; Zhang, L.; Faraj, Y.; Wang, W.; Ju, X. J.; Xie, R.; Chu, L. Y. A Simple Device Based on Smart Hollow Microgels for Facile Detection of Trace Lead(II) Ions. *ChemPhysChem* **2018**, *19* (16), 2025-2036.

(16) Memon, S. Q.; Hasany, S. M.; Bhanger, M. I.; Khuhawar, M. Y. Enrichment of Pb(II) ions using phthalic acid functionalized XAD-16 resin as a sorbent. *J. Colloid Interface Sci.* **2005**, *291* (1), 84-91.

(17) Liu, M.; Jia, L.; Zhao, Z.; Han, Y.; Li, Y.; Peng, Q.; Zhang, Q. Fast and robust lead (II) removal from water by bioinspired amyloid lysozyme fibrils conjugated with polyethyleneimine (PEI). *Chem. Eng. J.* **2020**, *390*, 124667.

(18) Pehlivan, E.; Altun, T. Ion-exchange of Pb^{2+}, Cu^{2+}, Zn^{2+}, Cd^{2+}, and N^{i2+} ions from aqueous solution by Lewatit CNP 80. *J. Hazard. Mater.* **2007**, *140* (1), 299-307.

(19) Gherasim, C.-V. I.; Bourceanu, G.; Olariu, R.-I.; Arsene, C. Removal of lead(II) from aqueous solutions by a polyvinyl-chloride inclusion membrane without added plasticizer. *J. Membr. Sci.* **2011**, *377* (1), 167-174.

(20) Qasem, N. A. A.; Mohammed, R. H.; Lawal, D. U. Removal of heavy metal ions from wastewater: a comprehensive and critical review. *npj Clean Water* **2021**, *4* (1), 36.

(21) Zhang, H.; Hodges, C. S.; Mishra, P. K.; Yoon, J. Y.; Hunter, T. N.; Lee, J. W.; Harbottle, D. Bio-Inspired Preparation of Clay–Hexacyanoferrate Composite Hydrogels as Super Adsorbents for Cs^{+}. *ACS Appl. Mater. Interfaces* **2020**, *12* (29), 33173-33185.

(22) Song, Y.; Jian, M.; Qiao, L.; Zhao, Z.; Yang, Y.; Jiao, T.; Zhang, Q. Efficient Removal and Recovery of Ag from Wastewater Using Charged Polystyrene-Polydopamine Nanocoatings and Their Sustainable Catalytic Application in 4-Nitrophenol Reduction. *ACS Appl. Mater. Interfaces* **2024**, *16* (5), 5834-5846.

(23) Wang, M.; Fu, M.; Li, J.; Niu, Y.; Zhang, Q.; Sun, Q. New insight into polystyrene ion exchange resin for efficient cesium sequestration: The synergistic role of confined zirconium phosphate nanocrystalline. *Chin. Chem. Lett.* **2024**, *35* (1), 108442.

(24) Zhang, X.; Razanajatovo, M. R.; Du, X.; Wang, S.; Feng, L.; Wan, S.; Chen, N.; Zhang, Q. Well-designed protein amyloid nanofibrils composites as versatile and sustainable materials for aquatic environment remediation: A review. *Eco-Environ. Health* **2023**, *2* (4), 264-277.

(25) Zhu, L.; Zhu, D.; Sheng, Y.; Xu, J.; Harbottle, D.; Zhang, H. Polydopamine-coated magnetic montmorillonite immobilized with potassium copper hexacyanoferrate for selective removal of Cs^{+} and its facile recovery. *Appl. Clay Sci.* **2022**, *216*, 106367.

(26) Liu, Y.-M.; Ju, X.-J.; Xin, Y.; Zheng, W.-C.; Wang, W.; Wei, J.; Xie, R.; Liu, Z.; Chu, L.-Y. A Novel Smart Microsphere with Magnetic Core and Ion-Recognizable Shell for Pb^{2+} Adsorption and Separation. *ACS Appl. Mater. Interfaces* **2014**, *6* (12), 9530-9542.

(27) Huang, Y.; Shen, Y.; Zhang, G.; Lu, P.; Wu, Z.; Tang, R.; Liu, J.; Wu, X.; Wang, C.; Zheng, H. Highly effective and selective removal of lead ions by polymer-grafted silica-coated acid-resistant magnetic chitosan composites. *Sep. Purif. Technol.* **2023**, *314*, 123561.

(28) Dong, Q.; Guo, X.; Huang, X.; Liu, L.; Tallon, R.; Taylor, B.; Chen, J. Selective removal of lead ions through capacitive deionization: Role of ion-exchange membrane. *Chem. Eng. J.* **2019**, *361*, 1535-1542.

(29) Hong, J.; Kang, L.; Shi, X.; Wei, R.; Mai, X.; Pan, D.; Naik, N.; Guo, Z. Highly efficient removal of trace lead (II) from wastewater by 1,4-dicarboxybenzene modified Fe/Co metal organic nanosheets. *J. Mater. Sci. Technol.* **2022**, *98*, 212-218.

(30) Huang, Y.; Zheng, H.; Hu, X.; Wu, Y.; Tang, X.; He, Q.; Peng, S. Enhanced selective

879 adsorption of lead(II) from complex wastewater by DTPA functionalized chitosan-coated magnetic
880 silica nanoparticles based on anion-synergism. *J. Hazard. Mater.* **2022**, *422*, 126856.
881 (31) Li, G.; Ye, J.; Fang, Q.; Liu, F. Amide-based covalent organic frameworks materials for
882 efficient and recyclable removal of heavy metal lead (II). *Chem. Eng. J.* **2019**, *370*, 822-830.
883 (32) Yang, Y.; Yan, Z.; Wang, L.; Meng, Q.; Yuan, Y.; Zhu, G. Constructing synergistic groups in
884 porous aromatic frameworks for the selective removal and recovery of lead(II) ions. *J. Mater. Chem. A*
885 **2018**, *6* (12), 5202-5207.
886 (33) Yoon, J. Y.; Zhang, H.; Kim, Y. K.; Harbottle, D.; Lee, J. W. A high-strength polyvinyl
887 alcohol hydrogel membrane crosslinked by sulfosuccinic acid for strontium removal via filtration. *J.*
888 *Environ. Chem. Eng.* **2019**, *7* (1), 102824.
889 (34) Ortega, L. M.; Lebrun, R.; Blais, J.-F.; Hausler, R. Removal of metal ions from an acidic
890 leachate solution by nanofiltration membranes. *Desalination* **2008**, *227* (1-3), 204-216.
891 (35) Gao, J.; Sun, S.-P.; Zhu, W.-P.; Chung, T.-S. Polyethyleneimine (PEI) cross-linked P84
892 nanofiltration (NF) hollow fiber membranes for Pb2+ removal. *J. Membr. Sci.* **2014**, *452*, 300-310.
893 (36) Zheng, J.; Li, Y.; Xu, D.; Zhao, R.; Liu, Y.; Li, G.; Gao, Q.; Zhang, X.; Volodine, A.; Van der
894 Bruggen, B. Facile fabrication of a positively charged nanofiltration membrane for heavy metal and
895 dye removal. *Sep. Purif. Technol.* **2022**, *282*, 120155.
896 (37) Hoang, M. T.; Pham, T. D.; Verheyen, D.; Nguyen, M. K.; Pham, T. T.; Zhu, J.; Van der
897 Bruggen, B. Fabrication of thin film nanocomposite nanofiltration membrane incorporated with
898 cellulose nanocrystals for removal of Cu(II) and Pb(II). *Chem. Eng. Sci.* **2020**, *228*, 115998.
899 (38) Zheng, J.; Zhang, X.; Li, G.; Fei, G.; Jin, P.; Liu, Y.; Wouters, C.; Meir, G.; Li, Y.; Van der
900 Bruggen, B. Selective removal of heavy metals from saline water by nanofiltration. *Desalination* **2022**,
901 *525*, 115380.
902 (39) Reinoso-Guerra, E.; Aristizabal, J.; Arce, B.; Zurob, E.; Dennett, G.; Fuentes, R.; Suescún, A.
903 V.; Cárdenas, L.; Rodrigues da Cunha, T. H.; Cabezas, R.; et al. Nanostructured Didymosphenia
904 geminata-based membrane for efficient lead adsorption from aqueous solution. *J. Environ. Chem. Eng.*
905 **2021**, *9* (4), 105269.
906 (40) Abdullah, N.; Gohari, R. J.; Yusof, N.; Ismail, A. F.; Juhana, J.; Lau, W. J.; Matsuura, T.
907 Polysulfone/hydrous ferric oxide ultrafiltration mixed matrix membrane: Preparation, characterization
908 and its adsorptive removal of lead (II) from aqueous solution. *Chem. Eng. J.* **2016**, *289*, 28-37.
909 (41) He, J.; Xiong, D.; Zhou, P.; Xiao, X.; Ni, F.; Deng, S.; Shen, F.; Tian, D.; Long, L.; Luo, L. A
910 novel homogenous in-situ generated ferrihydrite nanoparticles/polyethersulfone composite membrane
911 for removal of lead from water: Development, characterization, performance and mechanism. *Chem.*
912 *Eng. J.* **2020**, *393*, 124696.
913 (42) Jamshidi Gohari, R.; Lau, W. J.; Matsuura, T.; Halakoo, E.; Ismail, A. F. Adsorptive removal
914 of Pb(II) from aqueous solution by novel PES/HMO ultrafiltration mixed matrix membrane. *Sep. Purif.*
915 *Technol.* **2013**, *120*, 59-68.
916 (43) Zhao, D.; Yu, Y.; Chen, J. P. Treatment of lead contaminated water by a PVDF membrane that
917 is modified by zirconium, phosphate and PVA. *Water Res.* **2016**, *101*, 564-573.
918 (44) Su, R.; Ou, Q.; Wang, H.; Dai, X.; Chen, Y.; Luo, Y.; Yao, H.; Ouyang, D.; Li, Z.; Wang, Z.
919 Organic–inorganic composite modifiers enhance restoration potential of Nerium oleander L. to lead–
920 zinc tailing: application of phytoremediation. *Environ. Sci. Pollut. Res.* **2023**, *30* (19), 56569-56579.

(45) Ibrahim, N.; El Afandi, G. Phytoremediation uptake model of heavy metals (Pb, Cd and Zn) in soil using Nerium oleander. *Heliyon* **2020**, *6* (7), e04445.

(46) Trigueros, D.; Mingorance, M. D.; Rossini Oliva, S. Evaluation of the ability of Nerium oleander L. to remediate Pb-contaminated soils. *J. Geochem. Explor.* **2012**, *114*, 126-133.

(47) Izatt, R. M.; Pawlak, K.; Bradshaw, J. S.; Bruening, R. L. Thermodynamic and kinetic data for macrocycle interactions with cations and anions. *Chem. Rev.* **1991**, *91* (8), 1721-2085.

(48) Rounaghi, C.; Eshagi, Z.; Ghiamati, E. Study of the complex formation between 18C6 crown ether and Tl^{+}, Pb^{2+} and Cd^{2+} in binary non-aqueous solvents using differential pulse polarography. *Talanta* **1996**, *43* (7), 1043-1048.

(49) Biehl, M. P.; Izatt, R. M.; Lamb, J. D.; Christensen, J. J. Use of a Macrocyclic Crown Ether in an Emulsion (Liquid Surfactant) Membrane to Effect Rapid Separation of Pb^{2+} from Cation Mixtures. *Sep. Sci. Technol.* **1982**, *17* (2), 289-294.

(50) Ungaro, R.; El Haj, B.; Smid, J. Substituent effects on the stability of cation complexes of 4'-substituted monobenzo crown ethers. *J. Am. Chem. Soc.* **1976**, *98* (17), 5198–5202.

(51) Yagi, K.; Ruiz, J. A.; Sanchez, M. C. Cation binding properties of Polymethacrylamide Derivatives of Crown Ethers. *Makromol. Chem. Rapid Commun.* **1980**, *1* (4), 263-268.

(52) Gao, J.; Frisken, B. J. Influence of Secondary Components on the Synthesis of Self-Cross-Linked N-Isopropylacrylamide Microgels. *Langmuir* **2005**, *21* (2), 545-551.

(53) Ju, X.-J.; Liu, L.; Xie, R.; Niu, C. H.; Chu, L.-Y. Dual thermo-responsive and ion-recognizable monodisperse microspheres. *Polymer* **2009**, *50* (3), 922-929.

(54) Vijayakumar, B.; Takatsuka, M.; Kita, R.; Shinyashiki, N.; Yagihara, S.; Rathinasabapathy, S. Dynamics of the Poly(N-Isopropylacrylamide) Microgel Aqueous Suspension Investigated by Dielectric Relaxation Spectroscopy. *Macromolecules* **2022**, *55* (4), 1218-1229.

(55) Gandhi, A.; Paul, A.; Sen, S. O.; Sen, K. K. Studies on thermoresponsive polymers: Phase behaviour, drug delivery and biomedical applications. *Asian J. Pharm. Sci.* **2015**, *10* (2), 99-107.

(56) Boda, A.; Ali, S. M.; Shenoi, M. R.; Rao, H.; Ghosh, S. K. DFT modeling on the suitable crown ether architecture for complexation with Cs(+) and Sr(2)(+) metal ions. *J. Mol. Model.* **2011**, *17* (5), 1091-1108.

(57) Borhade, A. V.; Kshirsagar, T. A.; Dholi, A. G.; Agashe, J. A. Removal of Heavy Metals Cd^{2+}, Pb^{2+}, and Ni^{2+} From Aqueous Solutions Using Synthesized Azide Cancrinite, $Na_8[AlSiO_4]_6(N_3)_{2.4}(H_2O)_{4.6}$. *J. Chem. Eng. Data* **2015**, *60* (3), 586-593.

(58) Hayamizu, K.; Chiba, Y.; Haishi, T. Dynamic ionic radius of alkali metal ions in aqueous solution: a pulsed-field gradient NMR study. *RSC Adv.* **2021**, *11* (33), 20252-20257.

(59) He, J.; Mao, L.; Ma, X.; Hua, J.; Cui, Z.; He, B.; Pei, H.; Li, J. Highly-Efficient adsorptive separation of Cs^{+} from aqueous solutions by porous polyimide membrane containing Dibenzo-18-Crown-6. *Sep. Purif. Technol.* **2022**, *299*, 121757.

(60) Scotti, A.; Bochenek, S.; Brugnoni, M.; Fernandez-Rodriguez, M. A.; Schulte, M. F.; Houston, J. E.; Gelissen, A. P. H.; Potemkin, I. I.; Isa, L.; Richtering, W. Exploring the colloid-to-polymer transition for ultra-low crosslinked microgels from three to two dimensions. *Nat. Commun.* **2019**, *10* (1), 1418.

(61) Wang, J.; Guo, X. Adsorption kinetic models: Physical meanings, applications, and solving methods. *J. Hazard. Mater.* **2020**, *390*, 122156.

(62) Zhang, Y.; Wang, H.; Gao, K.; Huang, D.; Hou, L. a.; Yang, Y. Efficient removal of Cs(I) from water using a novel Prussian blue and graphene oxide modified PVDF membrane: Preparation, characterization, and mechanism. *Sci. Total Environ.* **2022**, *838*, 156530.

(63) Zheng, B.; Yin, J.; Zhu, L.; Zhou, B.; Shen, H.; Harbottle, D.; Hunter, T. N.; Sheng, Y.; Zhu, D.; Zhang, H. Thiol-rich and ion-imprinted alginate hydrogel as a highly adsorptive and recyclable filtration membrane for rapid and selective Sr(II) removal. *Chem. Eng. J.* **2023**, *465*, 142752.

(64) Zhang, H.; Kim, Y. K.; Hunter, T. N.; Brown, A. P.; Lee, J. W.; Harbottle, D. Organically modified clay with potassium copper hexacyanoferrate for enhanced Cs^+ adsorption capacity and selective recovery by flotation. *J. Mater. Chem. A* **2017**, *5* (29), 15130-15143.

(65) Yu, H.-R.; Hu, J.-Q.; Liu, Z.; Ju, X.-J.; Xie, R.; Wang, W.; Chu, L.-Y. Ion-recognizable hydrogels for efficient removal of cesium ions from aqueous environment. *J. Hazard. Mater.* **2017**, *323*, 632-640.

(66) Bai, R.; Zhang, L. Novel multifunctional membrane technology for visual detection and enhanced adsorptive removal of lead ions in water and wastewater. *Water Supply* **2011**, *11* (1), 113-120.

(67) Anitha, T.; Kumar, P. S.; Kumar, K. S.; Ramkumar, B.; Ramalingam, S. Adsorptive removal of Pb(II) ions from polluted water by newly synthesized chitosan–polyacrylonitrile blend: Equilibrium, kinetic, mechanism and thermodynamic approach. *Process Saf. Environ. Prot.* **2015**, *98*, 187-197.

(68) Feng, T.; Fan, Z.; Wu, S.; Chen, L.; Tian, Z. Electrospun polyacrylonitrile/hydroxyapatite composite nanofibrous membranes for the removal of lead ions from aqueous solutions. *New J. Chem.* **2022**, *46* (22), 10957-10966.

(69) Perez-Silva, I.; Paez-Hernandez, M. E.; Ibarra, I. S.; Camacho-Mendoza, R. L. Evaluation of the Hybrid Membrane of ZnO Particles Supported in Cellulose Acetate for the Removal of Lead. *Membranes (Basel)* **2023**, *13* (2).

(70) Yang, Y.; Zeng, L.; Lin, Z.; Jiang, H.; Zhang, A. Adsorption of Pb^{2+}, Cu^{2+} and Cd^{2+} by sulfhydryl modified chitosan beads. *Carbohydr. Polym.* **2021**, *274*, 118622.

(71) Xu, L.; Liu, Y.; Wang, J.; Tang, Y.; Zhang, Z. Selective adsorption of Pb^{2+} and Cu^{2+} on amino-modified attapulgite: Kinetic, thermal dynamic and DFT studies. *J. Hazard. Mater.* **2021**, *404*, 124140.

(72) Liu, Y.; Zhang, W.; Zhao, C.; Wang, H.; Chen, J.; Yang, L.; Feng, J.; Yan, W. Study on the synthesis of poly(pyrrole methane)s with the hydroxyl in different substituent position and their selective adsorption for Pb^{2+}. *Chem. Eng. J.* **2019**, *361*, 528-537.

(73) Zhang, S.; Ou, R.; Ma, H.; Lu, J.; Banaszak Holl, M. M.; Wang, H. Thermally regenerable metal-organic framework with high monovalent metal ion selectivity. *Chem. Eng. J.* **2021**, *405*, 127037.

(74) Liu, Z.; Luo, F.; Ju, X.-J.; Xie, R.; Sun, Y.-M.; Wang, W.; Chu, L.-Y. Gating membranes for water treatment: detection and removal of trace Pb^{2+} ions based on molecular recognition and polymer phase transition. *J. Mater. Chem. A* **2013**, *1* (34).

(75) Zhang, Y.; Kleine, T. S.; Carothers, K. J.; Phan, D. D.; Glass, R. S.; Mackay, M. E.; Char, K.; Pyun, J. Functionalized chalcogenide hybrid inorganic/organic polymers (CHIPs) via inverse vulcanization of elemental sulfur and vinylanilines. *Polym. Chem.* **2018**, *9* (17), 2290-2294.

(76) Kinuthia, G. K.; Ngure, V.; Beti, D.; Lugalia, R.; Wangila, A.; Kamau, L. Levels of heavy metals in wastewater and soil samples from open drainage channels in Nairobi, Kenya: community

health implication. *Sci. Rep.* **2020**, *10* (1), 8434.

1008